Nanoscale

Accepted Manuscript

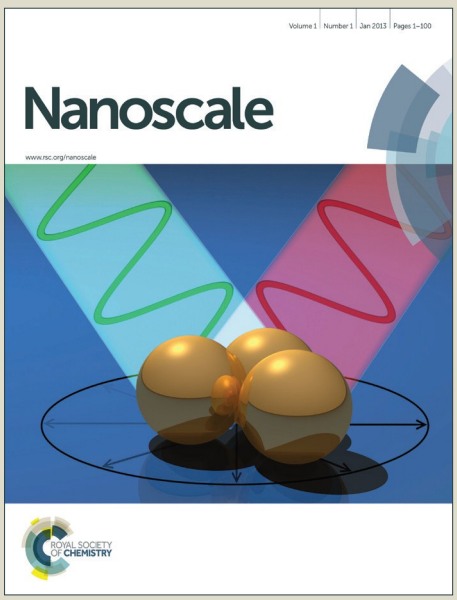

ROYAL SOCIETY OF CHEMISTRY

www.rsc.org/nanoscale

Doxorubicin-conjugated β-$NaYF_4$: Gd^{3+}/ Tb^{3+} multifunctional, phosphor nanorods: A multimodal, luminescent-magnetic probe for simultaneous optical, magnetoresonance imaging and an excellent pH-triggered anti-cancer drug delivery nanovehicle

Preeti Padhye[‡†], Aftab Alam[$], Suvankar Ghorai[$], Samit Chattopadhyay[$], Pankaj Poddar[‡†*]

‡Physical & Materials Chemistry Division, CSIR-National Chemical Laboratory, Pune - 411 008, India

†Academy of Scientific and Innovative Research, Anusandhan Bhawan, Rafi Marg, New Delhi - 110001, India

[$]National Center for Cell Sciences, Ganeshkhind, Pune-, 411 007, India

Abstract

Herein, we report the fabrication of a multifunctional nanoprobe based on highly monodispersed, optically and magnetically active, biocompatible, PEI-functionalized, highly crystalline β-$NaYF_4$: Gd^{3+}/ Tb^{3+} nanorods as an excellent multimodal optical/magnetic imaging tool and a pH-triggered intracellular drug delivery nanovehicle. The static and dynamic photoluminescent spectroscopy showed the presence of sharp emission peaks, with long lifetime (~ 3.5 milliseconds), suitable for optical imaging. The static magnetic susceptibility measurements at room temperature showed the strong paramagnetic signal (χ ~ 3.8 X 10^{-5} emu g^{-1} Oe^{-1}). The nuclear magnetic resonance (NMR) measurements showed fair T_1 relaxivity (r_1=1.14 $s^{-1}mM^{-1}$) and magnetoresonance imaging showed an enhanced T_1-weighted MRI images with increased concentrations of β-$NaYF_4$: Gd^{3+}/ Tb^{3+} making them

suitable for simultaneous magnetoresonance imaging. In addition, an anticancer drug, doxorubicin (DOX) was conjugated to the amine-functionalized β-$NaYF_4$: Gd^{3+}/ Tb^{3+} nanorods via a pH-sensitive hydrazone bond linkage enabling them as a pH-triggered, site-specific drug delivery nanovehicle for the DOX release inside the tumor cells. A comparison of *in vitro* DOX release studies at a normal physiological (pH 7.4) and acidic environment (pH 5.0) showed an enhanced DOX dissociation (~ 80 %) at pH 5.0. These multifunctional structures were also applied as an optical probe to confirm the conjugation of DOX and to monitor the DOX release via the fluorescence resonance energy transfer (FRET) mechanism. The DOX-conjugated β-$NaYF_4$: Gd^{3+}/ Tb^{3+} nanorods exhibited cytotoxic effect on MCF-7 breast cancer cells and their uptake by MCF-7 cells was demonstrated using confocal laser scanning microscopy and flow cytometry. A comparative cellular uptake of free DOX and DOX-conjugated β-$NaYF_4$: Gd^{3+}/ Tb^{3+} nanorods were studied in tumor microenvironment condition (pH 6.5) by confocal imaging, which showed the increased uptake of DOX-conjugated β-$NaYF_4$: Gd^{3+}/ Tb^{3+} nanorods. Thus, DOX-conjugated β-$NaYF_4$: Gd^{3+}/Tb^{3+} nanorods combining pH-triggered drug delivery, efficient luminescence and paramagnetic properties promise a potential multifunctional platform for cancer therapy, biodetection probe, optical and magnetoresonance imaging.

*Corresponding author Email: p.poddar@ncl.res.in

Keywords: Phosphor, multimodal imaging, FRET probe, magnetoresonance imaging, optical imaging, pH-triggered drug delivery.

Introduction

The widespread varieties of fluorescent probes have been used in bioimaging, biomedicine, diagnostics, theranostics, and multiplex sensing.[1-6] Recently, trivalent lanthanide (Ln^{3+})-ion-doped phosphors have emerged at the forefront as multifunctional nano probes, for a variety of biological applications. This is due to their unique optical features, arising from parity forbidden *f-f* transition, which are shielded by filled 5*s* and 5*p* orbitals. Compared to the conventional organic dyes, fluorophores and semiconductor quantum-dots (QDs), the lanthanide-ion-doped phosphors exhibit intriguing merits involving low-bandwidth, intense, tunable emission with long luminescent lifetime, large Stokes and anti-Stokes shift (down/upconversion), high photo-stability, low auto-florescence, photo-blinking and low toxicity.[7, 8] In addition, some lanthanide ions, specifically Gd^{3+} ions are highly paramagnetic due to the presence of seven unpaired electrons with large magnetic moments (~ 7.94 μ_B). Moreover, Gd^{3+} ions also possess longer electronic relaxation time, making them an excellent candidate as contrast agents for magnetoresonance imaging (MRI).[9, 10] These superior features relative to organic fluorescent dyes and QDs make the Ln^{3+}-ion-doped phosphors, a better alternative for various biological applications. Apart from biological applications, lanthanide-ion-doped phosphors have already proven to be highly technically important candidates in wide-ranging applications such as display devices, solid-state lasers, light emitting devices, optical telecommunication, solar cells, and catalysis. [11, 12]

An inorganic phosphor consists of a host lattice and optically active Ln^{3+} dopants, and the choice of appropriate host lattice, higher level of crystallinity play an important role in achieving a brighter phosphor. Inorganic fluorides, in particular $NaYF_4$, possess wide bandgap (~ 8 eV) and low phonon energy (~ 350 cm^{-1}) which is favorable for lower nonradiative losses and enhanced emission. In contrast the oxides phosphors usually show higher non-radiative losses.[13] The YVO_4 lattice has phonon energy of 880 cm^{-1}. In addition,

for tetragonal $NaGd(WO_4)_2$, tetragonal $GdVO_4$, and cubic Y_2O_3, the phonon thresholds of the host lattices are ~ 1000, ~ 880 and ~ 600 cm^{-1} respectively.[14-16] Therefore $NaYF_4$ based phosphors are considered as an excellent host matrix for down- and up-conversion luminescence processes.[17] The crystal structure of $NaYF_4$ exhibits two polymorphic forms- cubic (α-) and hexagonal (β-) phases. Among these phases, the hexagonal-phase of β-$NaYF_4$ is thermodynamically stable[18] which is desirable to achieve enhanced luminescence efficiency for various Ln^{3+} -ion-doped phosphors. Recently, we reported the high luminescence efficiency and efficient photocatalytic activity of β-$NaYF_4$:5 % Tb^{3+} phosphors.[19]

The development of multifunctional, hybrid nanoparticles, which integrate different functional properties into one entity, are promising as new research frontiers of multimodal bio-probes. The multifunctional nanoparticles with combined optical and magnetic properties can be immensely useful in multimodality imaging, where optical imaging provides the highest sensitivity for an *in vitro* cell imaging and MRI provide high penetration depth, excellent spatial resolution and anatomical information for *in vivo* imaging.[20] Usually, most of the conventional optically and magnetically active materials are composites that are produced by coupling traditional optically-active materials such as QDs and organic dyes with magnetic ones such as iron oxides etc. Recently, hybrids such as, dye-doped silica nanoparticles mixed with magnetite nanocrystals[21], Fe_3O_4@$NaLuF_4$:Yb/Er[22] and Fe_3O_4@LaF_3:Yb/Er[23] have been successfully synthesized for imaging. However, such hybrids suffer the disadvantage of photo-bleaching and toxicity of dyes, non-perseverance of particle size and complex synthesis processes with multiple steps. To overcome these drawbacks, single-phase, dual-function, superparamagnetic, Gd^{3+} containing inorganic nanocrystals have been developed as a new class of multimodal probes. Thus, inorganic crystals doped with optically active Ln^{3+} ions along with magnetic Gd^{3+} ions, not only bring

together the advantage of multimodal imaging/biodetection, but also effectively reduces the toxicity of free Gd^{3+} in rigid crystal environment.

The optical-magnetic nanoprobes are also expected to be used as drug-carriers for drug delivery and therapeutics. Doxorubicin (DOX) is the most established and commonly used chemotherapeutic anti-cancer drug. However, when the DOX is administered directly, it lacks targeting ability at tumor sites and shows minimal drug internalization.[24] According to the Warburg effect; increased anaerobic glycolysis results in lactic acid accumulation in cancer cells, which leads to lower extracellular pH (6.5 to 6.8) of many tumors.[25] Thus, the cellular uptake of weakly-basic drug- doxorubicin tend to reduce at low pH, which is in accordance with the pH partition theory.[26] The acidic extracellular microenvironment of tumors is therefore predicted to confer a degree of physiological resistance to weakly-basic drugs (e.g. doxorubicin) as well as it produces serious undesirable side effects such as cardiotoxicity etc.[24, 25] An imperative approach to overcome the toxicity and low cellular uptake concern of free doxorubicin drug is to develop the drug carrier system for tumor targeted drug delivery that can specifically respond to cancer cells with low pH values while staying inactive under normal physiological conditions.

The prime advantages of using nano sized particles in various bio-applications is due to their distinct optical, electronic, thermal and magnetic properties along with small size, and greater available surfaces for further modification.[27] In particular, for a drug delivery system the nano sized particles are beneficial as they possess longer circulation half-lives and enhanced permeability and retention effect (EPR) resulting in better drug accumulation at tumor site and consequent reduced side effects.[28] Herein, we designed and developed multifunctional nanorods, which can function as a dual-mode optical and magnetic bioprobe, integrated with the pH-triggered drug delivery capability. In particular, the nanorods are beneficial for intracellular drug delivery because the rod shaped structures possess larger

surface area and high surface energy. This leads to high drug conjugation efficiency and maximal drug loading capacity thereby making them as an efficient carrier for the drug delivery.[29] Thus, the amine functionalized β-$NaYF_4$:Gd^{3+}/Tb^{3+} nanorods were synthesized and utilized as luminescent/magnetic bioprobes, where the Tb^{3+} ions act as luminescent centers and Gd^{3+} ions render the paramagnetic property to the system. The DOX was then chemically conjugated with amine functionalized β-$NaYF_4$:Gd^{3+}/Tb^{3+} nanorods via a pH-sensitive hydrazone bond linkage (β-$NaYF_4$:Gd^{3+}/Tb^{3+}@ PEI–3-maleimidopropionic acid hydrazide (MPH)–DOX) for the pH-triggered drug delivery system. The photoluminescence and the magnetic properties were investigated. The drug release property, cytotoxicity and cellular uptake behavior were also studied in detail.

2. Materials and method

2.1 Materials

All the chemicals were of analytical grade and were used as-received without any further purification. Yttrium (III) nitrate hexahydrate (Y $(NO_3)_3.6H_2O$) (purity ≥ 99.89%), gadolinium (III) nitrate hexahydrate (Gd $(NO_3)_3.6H_2O$), terbium (III) nitrate hexahydrate (Tb $(NO_3)_3.6H_2O$) (purity ≥ 99.89%), polyethyleneimine branched polymer (average MW ~25,000), 1-ethyl-3-(3-dimethylaminopropyl) carbodiimide hydrochloride (EDC), 3-mercaptopropionic acid (MPA) and N-hydroxysuccinimide (NHS) were purchased from Sigma Aldrich Inc. Ammonium fluoride (NH_4F) and sodium chloride (NaCl) were received from Thomas Baker chemicals Pvt. Ltd. Doxorubicin was provided by Emcure Pharmaceuticals Ltd., Pune, India. The reagent 3-maleimidopropionic acid hydrazide (MPH) was obtained from Thermo Fisher Scientific India Pvt. Ltd. Deionized water was used throughout the experiments.

2.2 Synthesis

(a) One-pot synthesis of amine functionalized *β*-$NaYF_4$: 15%Gd/ 5% Tb

In a typical procedure, Y $(NO_3)_3.6H_2O$, Gd $(NO_3)_3.6H_2O$, and Tb $(NO_3)_3.6H_2O$ (0.2 M) were added to 10 mL NaCl solution (0.2 M). Under vigorous stirring, 20 mL of ethanol and 10 mL of PEI solution (5 wt %) were added to the above solution. After stirring of 30 min, NH_4F (0.5 M) was introduced into the above solution. After another agitation for several minutes, the solution was transferred into a stainless steel autoclave with Teflon liner of 80 mL capacity, sealed and heated at 200 °C for 24 h. After that, the autoclave was cooled to room temperature, and the resulting product was separated centrifugally and was washed with distilled water and absolute ethanol. Then, the product was dried under vacuum at 60 °C for 8 h.

(b) Synthesis of doxorubicin conjugated *β*-$NaYF_4$: 15%Gd^{3+}/ 5%Tb^{3+}

The doxorubicin was conjugated with *β*-$NaYF_4$: Gd^{3+}/Tb^{3+} via the pH-sensitive hydrazone bond to render the pH-triggered drug delivery following a modified method reported elsewhere.[30] NHS (27.6 mg), EDC (46.0 mg), and MPA (5.2 µL) were dissolved in 3 mL methanol. The mixture was stirred at room temperature for 5 h to form 3-mercaptopropanyl-N-hydroxysuccinimide ester (MP-NHS). PEI-functionalized *β*-$NaYF_4$: Gd^{3+}/Tb^{3+} (200.0 mg) was dispersed in 3 mL methanol, and the MP-NHS was added. The mixture was stirred for 12 h under nitrogen atmosphere, to form the thiolated PEI (*β*-$NaYF_4$: Gd^{3+}/Tb^{3+} @ PEI–SH). MPH (13.2 mg) was then added to the thiolated PEI *i.e.* *β*-$NaYF_4$: Gd^{3+}/Tb^{3+} @ PEI–SH to form PEI–MPH through the covalence of thiol and maleoyl. After 5 h of stirring, the methanol was evaporated and the solid (*β*-$NaYF_4$: Gd^{3+}/Tb^{3+} @ PEI– MPH) was hydrated and dialyzed against deionized water for 12 h. The freeze-dried *β*-$NaYF_4$: Gd^{3+}/Tb^{3+} @ PEI–MPH (50 mg) and DOX in excess were combined in methanol and allowed to react for 24 h while being protected from light to form the *β*-$NaYF_4$: Gd^{3+}/Tb^{3+}@

PEI–MPH–DOX conjugate (β-$NaYF_4$: Gd^{3+}/ Tb^{3+} - MPH – DOX). The reaction mixture was evaporated to dryness under reduced pressure, and the solid was dissolved in 5 mL water. This solution was dialyzed (MWCO 8000-1400) against deionized water at 4 °C and freeze-dried. The synthesis route is illustrated in Scheme 1.

2.3 Stability test of β-$NaYF_4$: Gd^{3+}/ Tb^{3+} nanorods and DOX-conjugated β-$NaYF_4$:Gd^{3+}/Tb^{3+}

To demonstrate the stability of the β -$NaYF_4$: Gd^{3+}/ Tb^{3+} nanorods and DOX-conjugated β-$NaYF_4$:Gd^{3+}/Tb^{3+}, the samples were incubated in Fetal Bovine Serum (FBS) at 37 °C for 3 days. The emission intensity of nanorods in serum was measured at λ_{ex} = 375 nm and the doxorubicin release was measured by excitation at 480 nm, emission maximum at 590 nm using fluorescence spectrophotometer at predetermined time intervals.

2.4 DOX loading and *In vitro* release of DOX from conjugates

The amount of DOX loaded on to the nanorods was calculated and determined by the characteristic DOX optical absorbance at 490 nm. 1 mg β-$NaYF_4$:Gd^{3+}/Tb^{3+} @PEI-MPH-DOX conjugate was dissolved in 1 mL water for the UV-vis measurement. The free DOX solutions of various concentrations were prepared, and the absorptions of the solutions were measured by UV-vis spectrophotometer to generate the calibration curve. The loading level was determined from the obtained calibration curve.

The DOX release studies were carried out in phosphate-buffered saline (PBS buffer) with different pH values (pH 7.4 and 5.0) at 37 °C. The β-$NaYF_4$:Gd^{3+}/Tb^{3+} @PEI-MPH-DOX conjugate was dispersed in 1mL of PBS and placed in a dialysis bag with a molecular weight cut-off of 3.5 kDa. The dialysis bags were then immersed in 10 mL of the release medium and kept in a shaker maintained at 100 rpm and 37 °C. One mL of the medium was sampled at selected time intervals, and replaced with fresh buffer solution. The amounts of released DOX were measured by UV-vis spectrophotometer.

To validate the loading of DOX on nanorods by chemical conjugation and pH-triggered release of DOX by cleavage of hydrazone bond, a control experiment was performed. The physical mixture of equal amount of β-$NaYF_4$: Gd^{3+}/ Tb^{3+} and DOX was dissolved in methanol and allowed to react for 24 h, in dark condition and further processed in the same way as for β-$NaYF_4$: Gd^{3+}/ Tb^{3+}-MPH-DOX synthesis. The loading of DOX was determined by the characteristic DOX optical absorbance at 490 nm. For DOX release studies, the physical mixture of equal amount of β-$NaYF_4$: Gd^{3+}/ Tb^{3+} and DOX was dissolved in methanol and allowed to react for 24 h, in dark condition. The reaction mixture was evaporated to dryness under reduced pressure. The solid was dispersed in PBS buffer with different pH values (pH 7.4 and 5.0) at 37 °C. The DOX release studies were then carried out in the similar way as for β-$NaYF_4$:Gd^{3+}/Tb^{3+} @PEI-MPH-DOX conjugate.

2.5 *In vitro* cytotoxicity of DOX-conjugated β-$NaYF_4$: Gd^{3+}/Tb^{3+} nanoparticles

2.5.1 Cell culture

The breast cancer cell line MCF-7 and NIH3T3 were cultured in Dulbeccòs modified Eagles medium (DMEM) supplemented with 10 % heat inactivated fetal bovine serum, penicillin (100 U/mL) and streptomycin (100 µg/mL) (Invitrogen Corporation, CA, USA) and incubated at 37 °C in 5 % CO_2 incubator (Thermo Scientific, NC).

2.5.2 Proliferation assay

The *in vitro* cell viability was assessed using 3-(4, 5-dimethylthiazol-2-yl)-2,5-diphenyltetrazolium bromide (MTT) proliferation assay in NIH3T3 and MCF-7 cells. The MCF-7 and NIH3T3 cells in monolayer culture were cultivated in DMEM media supplemented with 10 % heat inactivated fetal bovine serum, penicillin (100 U/mL) and streptomycin (100 µg/mL) (Invitrogen Corporation, CA, USA). Cells were trypsinized and plated at a density of ~ 20, 000 cells / well in 96-well plate. After ~ 24 h, cells were treated

with varying concentration of free DOX, β-$NaYF_4$:Gd^{3+}/Tb^{3+} nanorods and DOX-conjugated β-$NaYF_4$:Gd^{3+}/Tb^{3+}, and then cells were incubated in 5% CO_2 at 37 °C for 24 h. After the treatment, medium was removed and 10 μL of MTT (methylthiazole tetrazolium, 10 mg/mL) was added in each well and further incubated for 4 h at 37°C. Formazan crystals thus formed were solubilized in 100 μL iso-propanol and the absorbance of the MTT was measured at 570 nm with microplate reader (Theromo Multiskan go).

2.6 Cellular uptake of DOX-conjugated β-$NaYF_4$: Gd^{3+}/Tb^{3+} nanorods

Cellular uptake was examined using confocal laser scanning microscope (CLSM) and flow cytometry. MCF-7 breast cancer cells were seeded into chambered slide and allowed to grow for 24 h in DMEM medium containing 10 % FCS. On reaching 70 % cell confluence, the medium was replaced with 1 mL of fresh culture medium having pH 7.2 and pH 6.5 for cellular uptake study. The cells were treated with DOX-conjugated β-$NaYF_4$: Gd^{3+}/Tb^{3+} (β-$NaYF_4$: Gd^{3+}/ Tb^{3+} - MPH - DOX) nanorods (20 μg/mL) and incubated at 37 °C for 30 min, 2 h and 8 h, respectively. The cells were washed three times with PBS and fixed with 2 % paraformaldehyde at 37 °C for 10 min, and then rinsed with PBS three times again. After washing the cells thoroughly, the cells were overlaid with mounting medium containing DAPI (Sigma). The cover slips were placed on the slide and fluorescence images were recorded by using the fluorescence of DOX and β-$NaYF_4$: Gd^{3+}/Tb^{3+}, excited at 488 nm and 405 nm and emission was collected at 591 (red fluorescence) and 530 nm (green fluorescence) respectively. Similarly, the cells were treated with β-$NaYF_4$: Gd^{3+}/Tb^{3+} nanorods (20 μg/mL) and incubated at 37 °C, for 30 min and followed the same procedure as for DOX-conjugated β-$NaYF_4$: Gd^{3+}/Tb^{3+} for collecting green fluorescence from nanorods. The fluorescence emission (between 530 and 630 nm) was visualized by the confocal laser scanning microscope (Leica Microsystems and Carl Ziess, Germany). The cellular uptake of free DOX and DOX-conjugated β-$NaYF_4$: Gd^{3+}/ Tb^{3+} nanorods were also compared by

confocal microscopy. Free DOX and β-$NaYF_4$: Gd^{3+}/ Tb^{3+}-MPH-DOX nanorods were incubated with MCF-7 breast cancer cells at 37 °C for 30 min, 2 h and 8 h, respectively at pH 6.5 and followed the same above mention procedure. The fluorescence images were recorded by using the fluorescence of DOX excited at 488 nm and emission was collected at 591 (red fluorescence). For the flow cytometry studies, breast cancer MCF-7 cells were seeded in 6 well cell culture plates. The cells were then treated with the free DOX and DOX-conjugated β-$NaYF_4$: Gd^{3+}/Tb^{3+} nanorods for 4 h. To make single cell suspension, cells were trypsinized with 0.05 % trypsin-EDTA (Life Technologies) and washed with PBS. The cells were then resuspended in PBS buffer to a final concentration of 1×10^6 per mL for the flow cytometric analysis using a FACS Calibur flow cytometer (Becton Dickinson). The results were analyzed with Cell Quest software. The excitation wavelength and emission wavelength were 488 nm and 575 nm, respectively.

2.7 Spin relaxation measurement of β-$NaYF_4$: Gd^{3+}/Tb^{3+} nanorods and DOX-conjugated β-$NaYF_4$: Gd^{3+}/Tb^{3+} as Magnetic Resonance Imaging Contrast Agents.

For the solvent longitudinal relaxation times (T_1) measurements, the samples were dispersed in D_2O and the relaxivity values (r_1) were measured by a standard inversion-recovery pulse sequence on a Bruker Advance NMR spectrometer at 20 °C and 9.4 T (400 MHz). The ability of proton relaxation enhancement of β-$NaYF_4$: Gd^{3+}/Tb^{3+} is expressed by the term ionic relaxivity r_1, which is determined by the slope of following equation[31] in the units of mM^{-1} S^{-1}:

$$(1/T_1)_{obs} = (1/T_1)_d + r_1[M]$$

Where, $(1/T_1)_{obs}$ and $(1/T_1)_d$ are the observed values in the presence and absence of the paramagnetic species (β-$NaYF_4$: Gd^{3+}/Tb^{3+}) and [M] is the concentration of the β-$NaYF_4$: Gd^{3+}/Tb^{3+} nanorods.

To investigate the contrast enhancement effect, the T_1-weighted magnetic resonance images were acquired at RT using a 3 T Philips MR scanner using Standard Spin-Echo (SE) sequence. Various concentrations of samples (0, 0.05, 0.25, 0.5, 0.8 mM) in water were placed in a series of 2 mL tubes for T_1-weighted MRI images. The following parameters were adopted: repetition time (TR) = 500 ms, echo time (TE) = 9.4 ms, matrix size =128 pixels ×128 pixels, field of view (FOV) = 90, number of signal averages = 2, and slice thickness = 3 mm.

2.8 Characterization techniques

The phase purity and crystallinity of the as-prepared samples were characterized by X-ray diffraction (XRD) using a PANalytical X'PERT PRO instrument and the iron-filtered Cu-K_α radiation (λ = 1.5406 Å) in the 2θ range of 10-80° with a step size of 0.02°. To analyze the shape and size of the samples, field emission scanning electron microscopy (FESEM: Hitachi S-4200) was used. Energy-dispersive X-ray analysis (EDXA) of the samples was performed during FESEM measurements to obtain the elemental composition of the samples. The specific structure details, morphology, and size were obtained by using FEI Technai F30 high resolution transmission electron microscope (HRTEM) equipped with a super-twin lens (s-twin) operated at 300 keV accelerating voltage with Schottky field emitter source with maximum beam current (> 100 nA) and small energy spread (0.8 eV or less). The point-to-point resolution of the microscope is 0.20 nm and line resolution of 0.102 nm with a spherical aberration of 1.2 mm and chromatic aberration of 1.4 mm with 70 μm objective aperture size. The powder samples obtained were dispersed in ethanol and then drop-casted on carbon-coated copper TEM grids with 200 mesh and loaded to a single tilt sample holder.

The optical properties of the as-synthesized samples were investigated by a Jasco UV-vis-NIR (Model V570) dual beam spectrometer operated at a resolution of 2 nm. PL spectra were acquired using a Cary eclipse fluorescence spectrophotometer, equipped with a 400 W

Xe lamp as an excitation source and a Hamamatsu R928 photomultiplier tube (PMT) as a detector. Lifetime measurements were carried by using an Edinburgh Instruments FLSP 920 system, having a 60 W microsecond flash lamp as the excitation source. Around 30 mg sample was mixed with one ml methanol, made into a slurry and spread over a quartz plate and dried under ambient conditions and introduced into the sample chamber of the instrument prior to luminescence measurements. Fourier transform infrared spectrum (FTIR) was recorded by FTIR – 8300 Fourier transform infrared spectrophotometer (SHIMADZU) and Bruker FT-IR (ATR mode) spectrophotometer. Confocal laser scanning microscopy (CLSM) images were observed by Leica Microsystems and Carl Zeiss, Germany confocal microscope. The flow cytometry studies were performed by Calibur flow cytometer (Becton Dickinson) with an excitation wavelength of 480 nm. Magnetic property measurements of samples were performed using VSM (Vibrating Sample Magnetometer) attachment of Physical Property Measurement System (PPMS) from Quantum Design Inc., San Diego, CA, equipped with a 9 T superconducting magnet. For dc magnetic measurements, the samples were precisely weighed and packed inside a plastic sample holder which fit into a brass sample holder with negligible contribution in the overall magnetic signal. The M−H loops were collected at a rate of 75 Oe/s in a field sweep from −40 to 40 kOe at the vibrating frequency of 40 Hz.

3. Result and discussion

3.1 Characterization of β-$NaYF_4$: Gd^{3+}/Tb^{3+} and DOX-conjugated β-$NaYF_4$: Gd^{3+}/Tb^{3+}

Previous studies suggested that the cytotoxicity and cellular uptake efficiency of NPs can be largely affected by charge on the particles due to electrostatic interactions between nanoparticles and cell membrane.[32] Therefore, the surface coating on nanoparticles would play an important role in their cell internalization. Earlier studies also demonstrated that the positively charged, PEI-coated NPs significantly enhances cellular uptake in several human cell lines including cervical carcinoma (HeLa), glioblastoma (U87MG), and breast carcinoma

(MCF-7) cells.[32] Therefore, PEI was chosen to render the β-$NaYF_4$: Gd^{3+}/Tb^{3+} nanorods water solubility and amine functionalization.

X-ray diffraction analysis was used to characterize the phase purity, crystallinity and composition of β-$NaYF_4$: Gd^{3+}/Tb^{3+} nanorods. The X-ray diffraction pattern, as shown in Figure 1, exhibits sharp diffraction peaks that can be indexed to pure hexagonal-phase β-$NaYF_4$ (space group: $P6_3/m$). The absence of any other phase in XRD pattern indicates the high purity of as prepared samples. The calculated lattice parameters are a =5.9 Å, c =3.5 Å, which coincide well with the reported data (JCPDS no. 16-0334). Moreover, the sharpness of peaks in XRD pattern also indicates the high crystallinity of nanorods, which is beneficial to higher luminescence yield of phosphors, as the high crystallinity leads to less trap sites and subsequently gives strong emission. The size, shape and structure of the as-prepared nanorods were characterized by TEM and FESEM (Figure 2 and 3). TEM and FESEM images as shown in Figures 2 (a) and 3 (a), shows that the PEI capped β-$NaYF_4$: Gd^{3+}/Tb^{3+} crystals possess rod-shape with an average diameter ~ 60 nm and length of ~ 230 nm. It can be clearly seen that, the β-$NaYF_4$: Gd^{3+}/Tb^{3+} nanorods are highly uniform and monodispersed in nature. Even after conjugation of DOX on the surface, the nanoparticles showed good uniformity and monodispersity without any sign of aggregation (Figure 2 (b) and 3 (b)). The corresponding selected area electron diffraction patterns (SAED) and high resolution TEM images shown in Figure 2 (c, e) and (d, f) demonstrate that the as-synthesized β-$NaYF_4$: Gd^{3+}/Tb^{3+} nanorods and DOX-conjugated β-$NaYF_4$: Gd^{3+}/Tb^{3+} nanorods are highly crystalline in nature. Meanwhile, the lattice fringes with interplanar spacing of 0.3 nm and 0.2 nm were ascribed to (101) and (201) planes of β-$NaYF_4$: Gd^{3+}/Tb^{3+} nanorods and DOX-conjugated β-$NaYF_4$: Gd^{3+}/Tb^{3+} nanorods, respectively. Further, the elemental composition of the β-$NaYF_4$: Gd^{3+}/Tb^{3+} nanorods were determined by Energy Dispersive X-ray Analysis (EDX). As can be

seen by Figure 3 (c), all the elements including Na, Y, F, Gd and Tb can be detected in the spectrum.

The zeta potential and FTIR spectroscopy were employed to study the surface modification of β-$NaYF_4$: Gd^{3+}/Tb^{3+} nanorods by PEI and further conjugation of DOX on the β-$NaYF_4$: Gd^{3+}/Tb^{3+} nanorods. The ζ-potential of β-$NaYF_4$: Gd^{3+}/Tb^{3+} aqueous solution (pH=7) was measured to be + 57 mV, indicating the successful capping of PEI on the surface of β-$NaYF_4$: Gd^{3+}/Tb^{3+} nanorods. Owing to amino group capping on the surface, the nanorods were steadily dispersed in water to form a stable and optically transparent dispersion. The amino groups on the surface of nanorods were further verified by FTIR spectroscopy. The β-$NaYF_4$: Gd^{3+}/Tb^{3+} nanorods exhibited a sharp absorption band at 3626 cm^{-1} due to O-H stretching vibration. Meanwhile, absorption bands at 1385 cm^{-1} and 2830 cm^{-1} are attributed to the stretching vibrations of the C-N band symmetric stretching vibrations of C-H bond respectively. The IR-band centered at 1630 cm^{-1} was observed, which can be attributed to the N-H bending mode of amino group ($-NH_2$), and also a broad band at 3443 cm^{-1} is related to the N-H stretching vibration of amino group, thereby revealing the capping of PEI on the surface of nanorods.[31, 33] Further, when DOX was conjugated to the PEI coated nanorods via MPH, a feature peak at 1620 cm^{-1} appeared (Figure 4b) which can be assigned to –C=N– bond, resulting from reaction between hydrazide group of nanorods and carbonyl group at the 13-keto position of DOX. Moreover, the characteristic bands at 1135 cm^{-1} and 1380 cm^{-1} correspond to the absorption of DOX.[34] These results demonstrate that, the DOX molecules have been chemically conjugated to β-$NaYF_4$: Gd^{3+}/Tb^{3+} nanorods via hydrazone bond. Further, the conjugation of doxorubicin with β-$NaYF_4$: Gd^{3+}/Tb^{3+} nanorods was determined by the characteristic DOX absorption band at ~ 490 nm as shown by a comparison of UV-vis absorbance spectra of free DOX, β-$NaYF_4$: Gd^{3+}/Tb^{3+}-DOX conjugate and bare β-$NaYF_4$: Gd^{3+}/Tb^{3+} (Figure 5).

A comparison of the photoluminescence (PL) spectra of Tb^{3+} in β-$NaYF_4$: 5 % Tb^{3+} and β-$NaYF_4$: 15 % Gd^{3+}/ 5 % Tb^{3+} nanorods, when Tb^{3+} is excited directly (375 nm) and indirectly (273 nm) respectively, is shown in Figure 6 (a). It is evident that, in both the samples, the peak-positions in emission spectra remain similar, and the bands differ only in their relative intensities. The obtained emission spectra monitored at λ_{ex} = 273 nm, yielded intense green emissions in the regions of 480-680 nm, which are due to the $^5D_4 \rightarrow {}^7F_J$ (J = 3, 4, 5, 6) transitions of Tb^{3+} ions, respectively. Specifically, four prominent emission peaks centered at ~ 488, ~ 544, ~ 584, and ~ 619 nm, originates from the transitions of $^5D_4 \rightarrow {}^7F_6$, $^5D_4 \rightarrow {}^7F_5$, $^5D_4 \rightarrow {}^7F_4$, and $^5D_4 \rightarrow {}^7F_3$ respectively.[35] Among these transitions, the green emission $^5D_4 \rightarrow {}^7F_5$ at ~ 544 nm is the most intense emission, which corresponds to a magnetic dipole transition.

An important advantage of doping Gd^{3+} into the matrix is that, Gd^{3+} ions not only render paramagnetic property to the material but also act as sensitizer which enhances photoluminescence intensity via energy transfer from sensitizer Gd^{3+} to activator Tb^{3+} ion. It is well documented that, Gd^{3+} serves as an ideal UV sensitizer or intermediate to activate specific luminescence of Ln^{3+} ions such as Tb^{3+}, inducing green emissions in the visible region.[36] It is also evident from PL spectra in Figure 6 (b), emission intensity of β-$NaYF_4$: 15 % Gd^{3+}/ 5 % Tb^{3+} nanorods is greatly enhanced upon excitation at λ_{ex} = 273 nm as compared with λ_{ex} = 375 nm, which is the most effective direct excitation wavelength for Tb^{3+} ions.[19] We have also shown an comparative emission spectra of β-$NaYF_4$: 15 % Gd^{3+}/ 5 % Tb^{3+} and β-$NaYF_4$: 5 % Tb^{3+} (Figure 6 (a)), it can be clearly seen that β-$NaYF_4$: 15 % Gd^{3+}/ 5 % Tb^{3+} possess higher luminescence emission intensity, which is due to sensitization by Gd^{3+} ions. Previously, our group have studied the optical properties of Gd^{3+} ions and demonstrated that Gd^{3+} ions exhibit strong absorption band at 273 nm due to $^8S_{7/2} \rightarrow {}^6I_{11/2}$ transition in Gd^{3+} ions.[37] Thus, Gd^{3+} containing nanoparticles exhibit a very intense Ln^{3+} excitation band at 273

nm due to the $^8S_{7/2} \rightarrow {}^6I_J$ transition in Gd^{3+} ions followed by a non-radiative energy transfer to Ln^{3+} ions.[38] In the present β-$NaYF_4$: 15 % Gd^{3+}/ 5 % Tb^{3+} system, upon excitation at λ_{ex} = 273 nm Gd^{3+} ions absorb energy and subsequently efficiently transfer energy to neighbouring Tb^{3+} ions giving rise to high luminescence emission intensity.

The PL decay curves for the luminescence of Tb^{3+} in β-$NaYF_4$: 15 % Gd^{3+}/ 5 % Tb^{3+} nanorods are shown in Figure 7. This curve can be well fitted by a single exponential function as $I\ (t) = I_0 \exp(-t/\tau)$ where, I_0 is the initial emission intensity at t=0, τ is the 1/e lifetime of the emission centre. The lifetime for $^5D_4$ were detected at 544 nm for $^5D_4 \rightarrow {}^7F_5$ transition of Tb^{3+} by excitation at 273 nm and was determined to be 3.49 ms. The long luminescence lifetime is favorable for most of the biological applications, as the short lived fluorescence such as background fluorescence and autoflourescence can be easily suppressed which thus offers remarkably high signal-to-noise ratio.[7]

3.2 Controlled drug release and *in vitro* cytotoxicity

To evaluate the biocompatibility of the amine functionalized β-$NaYF_4$: 15 % Gd^{3+}/ 5 % Tb^{3+} nanorods, the standard MTT assay was performed on the NIH3T3 cells. The Figure 8 (a) shows the viability of NIH3T3 cells incubated with amine functionalized β-$NaYF_4$: 15 % Gd^{3+}/ 5 % Tb^{3+} nanorods at different concentrations for 24 h. It can be seen that, the β-$NaYF_4$: 15 % Gd^{3+}/ 5 % Tb^{3+} nanorods did not show any evident cytotoxicity to the NIH3T3 cells. The cell viabilities of almost 100 % were observed for a wide range of concentrations from 3.12 µg/mL to 200 µg/mL after incubation for 24 h. The cytotoxicity effect of free DOX and DOX-conjugated-β-$NaYF_4$: Gd^{3+}/ Tb^{3+} nanorods were checked in the NIH3T3 cells (Figure 8 (b)) and the results showed the potential decrease in the cytotoxicity of DOX-conjugated-β-$NaYF_4$: Gd^{3+}/ Tb^{3+}, indicating that toxic effects of DOX is reduced when conjugated with the β-$NaYF_4$: Gd^{3+}/ Tb^{3+}nanorods. These results coincide with the well established fact that the free DOX, when administered directly, confers adverse effects on the

normal cells. The reason behind the reduced toxicity of the DOX-conjugated-β-$NaYF_4$: Gd^{3+}/ Tb^{3+} nanorods in comparison to free DOX might be the protection of carbonyl group of DOX by β-$NaYF_4$: Gd^{3+}/ Tb^{3+}. It is believed that, doxorubicin cardiotoxicity is caused by doxorubicinol, which is the primary circulating metabolite of doxorubicin formed by the carbonyl reductase at the 13-keto position[39], thus the lack of a C-13 carbonyl moiety in DOX-conjugated-β-$NaYF_4$: Gd^{3+}/ Tb^{3+} prevents the formation of doxorubicinol, which itself promises reduced cardiotoxicity and adverse side effects as compared to free DOX delivery. The MTT results signify that, the amine functionalized β-$NaYF_4$: 15 % Gd^{3+}/ 5 % Tb^{3+} nanorods possess good biocompatibility as drug carriers and are also promising as fluorescent probes in bioimaging and other biological applications.

To demonstrate the cytotoxic effect of β-$NaYF_4$: Gd^{3+}/ Tb^{3+} - MPH - DOX nanorods *in vitro* against the cancer cells, the MTT assay of nanorods was performed against the MCF-7 cancer cells at pH 7.4. The Figure 9 shows the cell viabilities against β-$NaYF_4$: Gd^{3+}/ Tb^{3+} nanorods, DOX conjugated β-$NaYF_4$: Gd^{3+}/ Tb^{3+} nanorods and free DOX. Free DOX was taken as positive control to compare the cytotoxicity of β-$NaYF_4$: Gd^{3+}/ Tb^{3+} nanorods and DOX conjugate. The concentration of free DOX was set as the same as the DOX conjugated β-$NaYF_4$: Gd^{3+}/ Tb^{3+}. The samples were incubated with MCF-7 cancer cells for 24 h at 37 °C at different concentrations. The pure β-$NaYF_4$: Gd^{3+}/ Tb^{3+} nanorods without the DOX conjugation exhibited no cytotoxicity to the cancer cells even after 24 h of treatment at concentrations as high as 200 μg/mL. In contrast, both free DOX and DOX conjugated β-$NaYF_4$: Gd^{3+}/ Tb^{3+} nanorods exhibited an increasing inhibitory effect against the MCF-7 cancer cell proliferation with increasing concentration. The probable reason behind this may be attributed to the fact that the free DOX are small molecules, thus diffuse and spread faster into the cells, while DOX loaded nanocarriers have to be endocytosed to enter the cells. Thus,

when the concentration is higher, more DOX conjugated nanoparticles would be endocytosed to enter the cancer cells and release DOX inside to induce the cell death.[40, 41]

The stability of β-$NaYF_4$: Gd^{3+}/ Tb^{3+} nanorods and DOX-conjugated β-$NaYF_4$: Gd^{3+}/ Tb^{3+} nanorods was studied in fetal bovine serum (FBS) up to 3 days at 37 °C to mimic the physiological conditions. As shown in Figure S1 (a), the emission intensity of the β -$NaYF_4$: Gd^{3+}/ Tb^{3+} nanorods were hardly changed even over 60 h, indicating the significant stability of nanorods in the serum. The emission intensity is diminished by only 5 % which is not a significant drop. This small drop might be due to interaction of organic molecules present in the serum with the surface of nanorods. In the same way, the DOX-conjugated β -$NaYF_4$: Gd^{3+}/ Tb^{3+} nanorods were also stable in the FBS (Figure S1 (b)). After 60 h of incubation in FBS, the maximal release of doxorubicin was amounted to be only 7.6 %, indicating that doxorubicin is significantly stably bound to the nanorods under the physiological conditions. We further studied the drug loading and release abilities of the DOX-conjugated β-$NaYF_4$: 15 % Gd^{3+}/ 5 % Tb^{3+} nanorods through the pH-dependent cleavage of the hydrazone bond. The loading level of DOX in the nanorods is calculated to be 0.22 mg DOX/ β-$NaYF_4$: 15 % Gd^{3+}/ 5 % Tb^{3+} mg, which is determined by the characteristic DOX optical absorbance at 490 nm. The Figure 10 illustrates the DOX release profiles of β-$NaYF_4$:Gd^{3+}/Tb^{3+} -MPH-DOX conjugated nanorods in the PBS buffer solutions of different pH values (pH 7.4 and 5.0) at 37 °C. It can be clearly seen that, the DOX release rate at acidic pH i.e. at pH 5.0 is much faster than that at pH 7.4. Since the microenvironment of cancer cells is acidic (6.5 - 6.8), the pH-triggered drug delivery system can be considered as an smart drug carrier system in cancer therapy. The pH-triggered DOX release behavior in our system is acquired by conjugating DOX to PEI coated β-$NaYF_4$:Gd^{3+}/Tb^{3+} nanorods via pH sensitive hydrazone bond linkage (β-$NaYF_4$:Gd^{3+}/Tb^{3+} -MPH-DOX), which is quite stable at normal physiological conditions *i.e.* at neutral pH (pH 7.4), but cleaves quickly in the acidic environment (pH 4.5-5.0). As

observed from the Figure 10, DOX release rate markedly increased under the acidic conditions. More than ~ 52 % DOX released within 24 h and ~ 80 % of DOX released at the later stage *i.e.* at 65 h at acidic pH (pH 5); however at neutral pH (pH 7.4) nearly less than ~ 38 % DOX released within 24 h and, only ~ 54 % of DOX released in 65 h. To validate that the DOX was loaded on the nanorods by conjugation with hydrazone bond, but not simply by the physical absorption and the DOX release is taking place by cleavage of hydrazone bond in the acidic pH, we performed a control experiment where we combined DOX and β-$NaYF_4$: Gd^{3+}/ Tb^{3+} in methanol and allowed to react for 24 h, in dark condition and further processed in the same way as for β-$NaYF_4$: Gd^{3+}/ Tb^{3+}-MPH-DOX synthesis. The loading of the DOX on nanorods was checked by UV-vis spectrometer, but the characteristic signature absorbance band of the DOX (at 490 nm) was not observed. This indicates that the physical absorption of the DOX on the nanorod surfaces is negligible to render absorbance in the UV-vis spectrum. The release behaviour of DOX-nanorods incubated mixed solution was also studied. The Figure S2 demonstrates the release profile of DOX-nanorod mixture in PBS buffer solutions of different pH values (pH 7.4 and 5.0) at 37 °C. It can be clearly seen that, the unbound or non-specifically bound DOX (physically absorbed DOX if present), is rapidly diffused or released within 4 h, indicating uncontrolled release behavior of DOX. The release rate at different pH is also hardly affected. On the other hand, β-$NaYF_4$: Gd^{3+}/ Tb^{3+}-MPH-DOX showed controlled release kinetics (Figure 10) and minimal activity loss, which is important for targeted anticancer therapy. Further, we also confirmed the cleavage of hydrazone bond in DOX-conjugated β-$NaYF_4$: Gd^{3+}/ Tb^{3+} by FTIR (ATR mode). The time dependent FTIR study of DOX-conjugated β-$NaYF_4$: Gd^{3+}/ Tb^{3+} in PBS buffer of pH 5 at 37 °C as a function of time was performed. As can be seen from Figure S3, the feature band of hydrazone bond (–C=N–) at ~ 1620 cm^{-1} and band of DOX at ~ 1380 cm^{-1} found to be gradually depleted with time. A broad and weak band appeared at ~ 1585 cm^{-1} in the late stage (~ 52 h) is might be

due to presence of hydrazide group remained on the surface of nanorods after release of DOX.[34]

These results implicate that the loss of drug from β-$NaYF_4$: Gd^{3+}/ Tb^{3+} - MPH - DOX could be reduced during blood circulation at normal physiological environment (pH 7.4), while the drug release can be accelerated into the acidic environment and prominently release at lysosomes and consequently inside the cancer cells. Thereby, the DOX conjugated to β-$NaYF_4$: Gd^{3+}/ Tb^{3+} via pH-sensitive hydrazone bond may be effectively delivered and targeted to the tumor tissues and cancer cells by site-specific activation. It is well accepted that, as compared with the normal tissues, the tumors have acidic microenvironment, as tumor tend to accumulate high level of lactic acid due to anaerobic glycolysis.[25] Meanwhile, the cellular uptake and internalization of weakly basic drug doxorubicin is reduced at low pH due to pH gradient. Moreover, doxorubicin exhibit poor distribution, development of drug resistance and harmful side effects such as systemic toxicity, cardiotoxicity, suppression of immune system etc.[24, 26] Our present system β-$NaYF_4$: Gd^{3+}/ Tb^{3+} - MPH - DOX, where doxorubicin is conjugated to β-$NaYF_4$: Gd^{3+}/ Tb^{3+} via pH-sensitive hydrazone bond through MPH renders pH triggered targeted site activation DOX delivery by cleavage of hydrazone bond at pH 5.0 inside the tumor cells (scheme 2) and also significantly prevents the serious adverse effects and toxicity of DOX.

3.3 Fluorescence resonance energy transfer (FRET) between β-$NaYF_4$: Gd^{3+}/ Tb^{3+} nanoparticles and DOX

The DOX conjugated β-$NaYF_4$: Gd^{3+}/ Tb^{3+} nanorods can also be applied as an optical probe to confirm the conjugation of DOX to β-$NaYF_4$: Gd^{3+}/ Tb^{3+} and to monitor the release of DOX via fluorescence resonance energy transfer, also termed as Forster resonance energy transfer (FRET) between β-$NaYF_4$: Gd^{3+}/ Tb^{3+} and DOX. The luminescence of β-$NaYF_4$: Gd^{3+}/ Tb^{3+} are quenched by DOX through energy transfer between FRET pair. As shown in

Figures 11 (a, b), the broad absorbance of DOX occurs between 450 nm to 550 nm, which overlaps the green emission of β-$NaYF_4$: Gd^{3+}/ Tb^{3+} at 488 nm and 540 nm. This spectral overlap enables the quenching of luminescence intensity of β-$NaYF_4$: Gd^{3+}/ Tb^{3+} after the reaction with DOX (Figure 11 (c)). We can also monitor the release of DOX by FRET mechanism. It is well demonstrated that, the FRET process results from dipole-dipole interactions and thus FRET is extremely sensitive to distance between donor and acceptor, consequently FRET can effectively occur only when the donor and acceptor are in close proximity.[42, 43] At pH 5.0, DOX has been released from β-$NaYF_4$: Gd^{3+}/ Tb^{3+} nanorods by cleavage of hydrazone bond and thus diffused away from the nanorods, which cease the FRET process. Therefore, we can register the increase in luminescence intensity of β-$NaYF_4$: Gd^{3+}/ Tb^{3+} with the gradual release of DOX. This is established by studying the photoluminescence spectra of DOX-conjugated β-$NaYF_4$: Gd^{3+}/ Tb^{3+} in PBS buffer of pH 5 at 37 °C as a function of time. As shown in Figure 12 (a), the luminescence of β-$NaYF_4$: Gd^{3+}/ Tb^{3+} has gradually recovered along with the release of DOX. Moreover, the fluorescence of DOX conjugated β-$NaYF_4$: Gd^{3+}/ Tb^{3+} have also been considerably quenched as compare to free DOX, when excited at 490 nm (Figure 12 (b)). In previous studies, it has been reported that, the fluorescence of DOX has been quenched due to hydrophobic interaction between the hydrocarbon chains of oxidized oleic acid on the nanoparticle surface and the anthraquinone ring of doxorubicin molecule.[44] In another report, the quenching effect in DOX-NP conjugate was observed due to the intermolecular interactions between DOX molecules after its dense packing on the surface of nanoparticles.[45] In present work, interaction between hydrazide group on nanorod's surface and 13- C carbonyl group of might have resulted in quenching of DOX fluorescence. Further, a detailed mechanism is required to be studied in future.

3.4 Cell uptake

The cell uptake process has been measured using confocal laser scanning microscopy (CLSM) after incubating β-$NaYF_4$: Gd^{3+}/ Tb^{3+}-MPH-DOX nanorods with MCF-7 breast cancer cells in different time period. The green emission is from β-$NaYF_4$: Gd^{3+}/ Tb^{3+} nanorods and red fluorescence is from DOX. In the initial 30 min time period (Figures 13), very few nanorods could be taken up by the MCF-7 cells. It can be clearly seen that the accumulation of the red emitting particles (red fluorescence from DOX) are apparently increased after incubation of 2 h. After prolong incubation period of 8 h, increased fluorescence from DOX have been appeared inside the cells. Similarly, green emission was increased with prolonging time. Confocal laser scanning microscopy (CLSM) images of MCF-7 cancer cells incubated with β-$NaYF_4$: Gd^{3+}/ Tb^{3+} nanorods are also shown in Figure S4. The green emission signals observed from β-$NaYF_4$: Gd^{3+}/ Tb^{3+} (Figure 13 and S4), demonstrates that these could also be used as an optical probe for imaging. These results indicated the efficient internalization of β-$NaYF_4$: Gd^{3+}/ Tb^{3+}-MPH-DOX nanorods by the MCF-7 breast cancer cells. The red fluorescence from the released DOX was observed in both cytoplasm and the cell nucleus (Figure S5). CSLM images clearly shown time course increase in the fluorescence intensity of doxorubicin-conjugated β-$NaYF_4$: Gd^{3+}/ Tb^{3+}which correlates to release of DOX inside the cell. Here, we predict that more doxorubicin release is due to the internalization of β-$NaYF_4$: Gd^{3+}/ Tb^{3+}-MPH-DOX nanoparticles in different acidic compartments of cells such as endosomes and lysosomes where there is low pH ranging from (pH 4 - 6). The acidic environment cleaves the pH-sensitive hydrazone bond to enable the release of doxorubicin.

Further to establish the benefit of DOX-conjugated β-$NaYF_4$: Gd^{3+}/ Tb^{3+} nanorods in targeting cancer cells, pH dependent uptake of free DOX and DOX-conjugated β-$NaYF_4$: Gd^{3+}/ Tb^{3+} nanorods in MCF-7 breast cancer cell was further studied. We compared the

cellular uptake of free DOX and DOX-conjugated β-$NaYF_4$: Gd^{3+}/ Tb^{3+} nanorods by confocal microscopy. Free DOX and β-$NaYF_4$: Gd^{3+}/ Tb^{3+}-MPH-DOX nanorods were incubated with MCF-7 breast cancer cells for different time period at pH 6.5, which mimic the tumor microenvironment where the pH is between 6.5 - 6.8. As can be clearly seen from Figure 14, the red fluorescence from DOX, i.e. the accumulation of DOX is increased when incubated with DOX-conjugated β-$NaYF_4$: Gd^{3+}/ Tb^{3+} nanorods as compared to free DOX at pH 6.5. The objective behind designing DOX-conjugated β-$NaYF_4$: Gd^{3+}/ Tb^{3+} (β-$NaYF_4$: Gd^{3+}/ Tb^{3+}-MPH-DOX) based drug delivery system is the sustained release of weakly basic DOX in an ideal acidic tumor microenvironment, as the native DOX cannot be effectively taken up at acidic condition. It can be clearly seen that (Figure 14) DOX-conjugated β-$NaYF_4$: Gd^{3+}/ Tb^{3+} could be able to work more effectively than free DOX at low pH. This indicates that in the present system, β-$NaYF_4$: Gd^{3+}/ Tb^{3+} nanorods when conjugated to DOX via hydrazone bond increase the cellular uptake and delivery of DOX in the tumor cells.

Flow cytometry analysis of free DOX and DOX-conjugated β-$NaYF_4$: Gd^{3+}/ Tb^{3+} nanorods was further performed to confirm the uptake of DOX-conjugated β-$NaYF_4$: Gd^{3+}/ Tb^{3+} nanorods by the MCF-7 cells by means of measuring the fluorescence intensities of DOX in the cells. The β-$NaYF_4$: Gd^{3+}/ Tb^{3+}-MPH-DOX nanorods were used to deliver DOX to the cells. Thus, the cell uptake degree of the β-$NaYF_4$: Gd^{3+}/ Tb^{3+}-MPH-DOX conjugate can be quantified using flow cytometry by determining the red fluorescence emitted from the released DOX. For flow cytometry analysis, the cells were seeded and incubated with free DOX and β-$NaYF_4$: Gd^{3+}/ Tb^{3+}-MPH-DOX nanorods for 4 h. Single cell suspension were prepared and the fluorescence intensity of the control cells and the sample cells were measured. It can be clearly noted that, the amount of red fluorescence in sample cells (Figures 15 c, d and e, f) is much higher than the control cells (Figure 15 a, b). The flow cytometry results further confirmed that the β-$NaYF_4$: Gd^{3+}/ Tb^{3+}-MPH-DOX nanorods were

taken up by MCF-7 breast cancer cells. Therefore, the DOX conjugated β-$NaYF_4$: Gd^{3+}/ Tb^{3+} nanorods enter and get internalized by the cancer cells and assemble into the cytoplasm. Meanwhile, the DOX is released from β-$NaYF_4$: Gd^{3+}/ Tb^{3+} nanorods by the cleavage of hydrazone bond into the nucleus and, consequently kill the cancer cells by causing DNA damage by intercalation, inhibition of nucleic acid and protein synthesis and disruption of DNA repair enzymes.[46, 47]

3.5 Magnetic measurements

In addition to the excellent luminescence property, the amine functionalized β-$NaYF_4$: 15 % Gd^{3+}/ 5 % Tb^{3+} nanorods as well as DOX-conjugated β-$NaYF_4$: 15 % Gd^{3+}/ 5 % Tb^{3+} nanorods exhibited paramagnetism (Figure 16), which makes these nanorods suitable as dual modality optical-magnetic multifunctional nanophosphors. The Figures 16 (a) and (b), shows the room temperature (RT) magnetization (M) as a function of the applied magnetic field (H) for amine functionalized β-$NaYF_4$: 15 % Gd^{3+}/ 5 % Tb^{3+} nanorods and DOX-conjugated β-$NaYF_4$: 15 % Gd^{3+}/ 5 % Tb^{3+} nanorods respectively. These nanorods exhibit typical paramagnetic behavior at 300 K and applied field in range from - 40 to + 40 kOe. The paramagnetic properties of the Gd^{3+} ions arise from seven unpaired inner 4f electrons, which are closely bound to the nucleus and effectively shielded from crystal field by the outer $5s^2$ $5p^6$ shell electrons. Thus, it prohibits sufficient overlap of the orbital's associated with the partially filled 4f electrons shells of the Gd^{3+} ions necessary for ferromagnetism. It turns out that the magnetic moments associated with the Gd^{3+} ions are all localized and non-interacting giving rise to paramagnetism.[48]

The room temperature magnetic mass susceptibility of amine functionalized β-$NaYF_4$: 15 % Gd^{3+}/ 5 % Tb^{3+} nanorods and DOX-conjugated β-$NaYF_4$: 15 % Gd^{3+}/ 5 % Tb^{3+} nanorods are 3.83 X 10^{-5} emu g^{-1} Oe^{-1} and 2.49 X 10^{-5} emu g^{-1} Oe^{-1}, respectively.

Furthermore, the magnetization of β-$NaYF_4$: 15 % Gd^{3+}/ 5 % Tb^{3+} nanorods and DOX-conjugated β-$NaYF_4$: 15 % Gd^{3+}/ 5 % Tb^{3+} nanorods is ~ 0.76 emu g^{-1} and ~ 0.49 emu g^{-1}, respectively at 20 k Oe. These values are close to the reported values of nanoparticles used very frequently for bioseperation and also successfully used as T_1-MRI contrast agent.[33, 49] To further demonstrate the potential application of β-$NaYF_4$: Gd^{3+}/ Tb^{3+} nanorods as a MRI contrast agent, a series of β-$NaYF_4$: Gd^{3+}/ Tb^{3+} nanorods and DOX-conjugated β-$NaYF_4$: Gd^{3+}/ Tb^{3+} nanorods with different molar concentrations were used for the ionic longitudinal relaxivity (r_1) study using the NMR spectrometer. From the slope of plot of $1/T_1$ verses Gd^{3+} concentration (Figure 16 (c, d)), the relaxation rate $1/T_1$ (r_1) value for the β-$NaYF_4$: Gd^{3+}/ Tb^{3+} nanorods and the DOX-conjugated β-$NaYF_4$: Gd^{3+}/ Tb^{3+} were determined to be 1.41 s^{-1} mM^{-1} and 1.02 s^{-1} mM^{-1} respectively. Figure 16 (e) and (f) shows typical T_1-weighted MRI images of β-$NaYF_4$: Gd^{3+}/ Tb^{3+} nanorods and DOX-conjugated β-$NaYF_4$: Gd^{3+}/ Tb^{3+}. The T_1-weighted imaging for the samples was performed for 4 different concentrations varying from 0.05 to 0.8 mM (water for the reference signal) on a 3 T MR scanner. With the increasing concentration, the T_1-weighted MRI signal intensity was clearly enhanced, thus showed positive enhancement effect, demonstrating that the β-$NaYF_4$: Gd^{3+}/ Tb^{3+} nanorods might be an effective T_1-MRI contrast agent.

Therefore, the as-prepared amine functionalized β-$NaYF_4$: 15 % Gd^{3+}/ 5 % Tb^{3+} are multifunctional nanorods with high luminescence properties and intrinsic paramagnetism, thus, these may find useful applications in bio-imaging, bio-separation and magnetic resonance imaging.

4. Summary

In summary, we have developed multi-modal probe based on PEI capped β-$NaYF_4$: Gd^{3+}/Tb^{3+}, which possess excellent photoluminescence as well as paramagnetic properties, making them suitable for optical bioimaging and MRI applications. A widely used anti-

cancer drug, doxorubicin, was conjugated to PEI capped β-$NaYF_4$: Gd^{3+}/Tb^{3+} via pH-sensitive hydrazone bond linkage. This system displays the pH-triggered drug delivery system, where the doxorubicin is released by cleavage of hydrazone bond in the acidic microenvironment of tumor, which reduces the side-effects of chemotherapeutics. The pH dependent *in vitro* DOX release studies shown that, the DOX release at acidic pH are significantly faster than at pH 7.4. Furthermore, the luminescence quenching of β-$NaYF_4$: Gd^{3+}/Tb^{3+} by DOX due to FRET mechanism can be applied as optical probe to confirm the DOX conjugation and monitor the DOX release. Cell toxicity assays revealed that the PEI capped β-$NaYF_4$: Gd^{3+}/Tb^{3+} possess very low toxicity. Meanwhile, the *in vitro* cytotoxicity of DOX- conjugated β-$NaYF_4$: Gd^{3+}/Tb^{3+} on MCF-7 cancer cells exhibited comparable cellular toxicity with respect to free DOX. The cellular uptake of DOX-conjugated β-$NaYF_4$: Gd^{3+}/Tb^{3+} by MCF-7 cells are established by confocal laser scanning microscopy study. The cellular uptake of DOX-conjugated β-$NaYF_4$: Gd^{3+}/Tb^{3+} by MCF-7 cells were enhanced compared to free DOX at pH 6.5, which mimic tumor microenvironment. Along with high luminescence efficiency, the magnetic mass susceptibility of β-$NaYF_4$: Gd^{3+}/Tb^{3+} and longitudinal relaxivity (r_1) were close to those of materials reported for MRI and bio-separation. It is expected that DOX-conjugated β-$NaYF_4$: Gd^{3+}/Tb^{3+} combining pH-triggered drug delivery, efficient luminescence and paramagnetic properties promises as potential multifunctional platform for cancer theranostics, biodetection probe and imaging.

Acknowledgement

Pankaj Poddar acknowledges the Centre for Excellence in Surface Science at the CSIR-National Chemical Laboratory, and network project Nano-Safety, Health & Environment (SHE) funded by the Council of Scientific and Industrial Research (CSIR), India, and the Department of Science & Technology (DST), India through and Indo-Israel grant to develop materials for solar-voltaic energy devices (DST/INT/ISR/P-8/2011). Authors

acknowledge Dr. V. Sudarshan, Chemistry division, Bhabha Atomic Research Centre, Mumbai, for luminescence lifetime measurements. Authors also acknowledge Dr. P.R. Rajmohanan and Ms. Kavya, NMR group, CSIR-National Chemical Laboratory, Pune, for the help with NMR measurements. Preeti Padhye acknowledges the support from the University Grant Commission (UGC), India for providing the Senior Research Fellowship (SRF).

References

1. J. H. Lee, Y.M. Huh, Y. W. Jun, J. W. Seo, J.T. Jang, H. T. Song, S. Kim, E. J. Cho, H. G. Yoon, J. S. Suh and J. Cheon, *Nature Medicine* ., 2006, **13**, 95-99.
2. S. K. Bhunia, A. Saha, A. R. Maity, S. C. Ray and N. R. Jana, *Scientific Reports*., 2013, **3**, 1-7.
3. Q. Zhao, C. Huanga and F. Li, *Chem. Soc. Rev*., 2011, **40**, 2508-2524.
4. D. GeiBler, L. J. Charbonniere, R. F. Ziessel, N. G. Butlin, H.G. Lohmannsroben, and N. Hildebrandt, *Angew. Chem. Int. Ed*., 2010, **49**, 1396-1401.
5. L. Shao, Y. Gao and F. Yan, *Sensors*., 2011, **11**, 11736-11751.
6. A. Thibon and V. C. Pierre, *Anal Bioanal Chem*., 2009, **394**,107–120.
7. Y. Liu, D. Tu, H. Zhuab and X. Chen, *Chem. Soc. Rev.,* 2013, **42**, 6924-6958.
8. Y. Liu, D. Tu, H. Zhu, E. Ma and X. Chen, *Nanoscale*, 2013, **5**, 1369-1384.
9. H. B. Na, I. C. Song, and T. Hyeon, *Adv. Mater*., 2009, **21**, 2133-2148.
10. K. N. Raymond and V. C. Pierre, *Bioconjugate Chem*., 2005**, 16**, 3-8.
11. J. W. Stouwdam and F. C. J. M. van Veggel, *Nano Lett*., 2002, **2**, 733-737.
12. G. Wang, Q. Peng and Y. Li, *ACCOUNTS OF CHEMICAL RESEARCH*., 2011, **44** 322-332.
13. F. Wang and X. Liu, *Chem. Soc. Rev.,* 2009, **38**, 976-989.
14. J. H. Huang, X.H. Gong, Y. J. Chen, Y.F. Lin, J.S. Liao, X.Y. Chen, Z.D. Luo, and Y. D. Huang, *Applied Physics B* , 2007, **89**, 73-80.
15. A. A. Kaminskii, O. Lux, H. Rhee, H.J. Eichler, K. Ueda, H. Yoneda, A. Zhao, B. Shirakawa, J. Chen, J. Dong, and J. Zhang, *Laser Phys. Lett* ., 2012, **9**, 879-887.
16. J. A. Capobianco, F. Vetrone, and J. C**.** Boyer, *J. Phys. Chem. B.,* 2002, **106**, 1181-1187.

17. C. Li, C. Zhang, Z. Hou, L. Wang, Z. Quan, H. Lian, and J. Lin, *J. Phys. Chem. C*., 2009, **113**, 2332-2339.

18. C. Li, Z. Quan, J. Yang, P. Yang, and J. Lin, *Inorganic Chemistry*., 2007, **46**, 6329-6337.

19. P. Padhye and P. Poddar, *J. Mater. Chem. A*., 2014, **2**, 19189-19200.

20. R. Kumar, M. Nyk, T. Y. Ohulchanskyy, C.A. Flask, and P. N. Prasad, *Adv. Funct. Mater*., 2009, **19**, 853-859.

21. J. E. Lee, N. Lee, H. Kim, J. Kim, S. H. Choi, J. H. Kim, T. Kim, I. C. Song, S.Pyo Park,W. K. Moon, and T. Hyeon, *J. AM. CHEM. SOC*., 2010,**132**, 552-557.

22. X. Zhu, J. Zhou, M. Chen, M. Shi, W. Feng, F. Li, *Biomaterials*., 2012, **33**, 4618-4627.

23. L. Zhang, Y.S. Wang, Y. Yang, F. Zhang, W. F. Dong, S. Y. Zhou, W. H. Pei, H. D. Chen and H. B. Sun, *Chem. Commun*., 2012, 48, 11238-11240.

24. A. Madhusudhan , G. B. Reddy , M. Venkatesham, G.Veerabhadram, D. A. Kumar, S.Natarajan, M. Y. Yang, A.Hu, and S. S. Singh, *Int. J. Mol. Sci.,* 2014, **15**, 8216-8234.

25. K. Newell, A. Franchi, J. Pouyssegur, and I. Tannock, *Proc. Natl. Acad. Sci. USA*., 1993, **90**, 1127-11231.

26. P. Swietach, A. Hulikova, S.Patiar, R. D. Vaughan-Jones, A. L. Harris, *PLoS ONE*; 2012, **7**, 1-9.

27. P.R. Sajanlal, T. S. Sreeprasad, A. K. Samal, and T. Pradeep, *Nano Reviews*., 2011, **2**, 5883.

28. C. M. J Hu, S. Aryal, and L. Zhang , *Therapeutic Delivery*., 2010, **1**, 323-334.

29. R. Venkatesan, A. Pichaimani, K. Hari, P.K. Balasubramanian, J. Kulandaivel, and K. Premkumar, *J. Mater. Chem. B*., 2013, **1**, 1010-1018.

30. D. W. Dong, S.W. Tong, X. R. Qi, *J Biomed Mater Res Part A*., 2013, **101**, 1336-1344.

31. Q. Ju, D. Tu, Y. Liu, R. Li, H. Zhu, J. Chen, Z. Chen, M. Huang, and X. Chen, *J. Am. Chem. Soc*., 2012, **134**, 1323-1330.

32. J. Jin, Y. J. Gu, C. W. Yin Man, J. Cheng, Z. Xu, Y. Zhang, H. Wang, V. H.Y. Lee, S. H. Cheng, and W. T. Wong, *ACS Nano.,* 2011, **5**, 7838-7847.

33. S. Zeng, M. K. Tsang, C. F. Chan, K. L. Wong, B. Fei and J. Hao*, Nanoscale*., 2012, **4**, 5118-5424.

34. F. H. Chen, L. M. Zhang, Q. T. Chen, Y. Zhang and Z. J. Zhang, *Chem. Commun*., 2010, **46**, 8633-8635.

35. Z. Hao, J.Zhang, X. Zhang, S. Lu, and X. Wang, *Journal of The Electrochemical Society.,* 2009, **156,** 193-196.

36. Y. Liu , D. Tu , H. Zhu , R. Li , W. Luo , and X. Chen, *Adv. Mater.*, 2010, **22**, 3266-71.

37. A. Jaiswal, R. Das, S. Adyanthaya, P. Poddar, *J Nanopart Res*., 2011, **13**,1019-10127.

38. M. Banski, A. Podhorodecki, J. Misiewicz, M. Afzaal, A. L. Abdelhady and P. O'Brien, *J. Mater. Chem. C*., 2013, **1**, 801-807.

39. M. Shi, K. Ho, A. Keating, and M. S. Shoichet, *Adv. Funct. Mater*., 2009, **19**, 1-8.

40. D. Yang, X. Yang, P. Ma, Y. Dai, Z. Hou, Z. Cheng, C. Li, J. Lin, *Biomaterials*., 2012, **34**, 1601-1612.

41. X. Li, Z. Hou, P. Ma, X. Zang, C. Li, Z. Cheng, J. Lian, J. Lin, *RSC Adv*., 2013, 3, 8517–8526.

42. A. R. Clapp, I. L. Medintz, J. M. Mauro, B. R. Fisher, M. G. Bawendi, and H. Mattoussi, *J. AM. CHEM. SOC*., 2004, **126**, 301-310.

43. A. A. Deniz, M. Dahan, J. R. Grunwell, T. Ha, A. E. Faulhaber, D. S. Chemla, S. Weiss and P. G. Schultz, *Proc. Natl. Acad. Sci. USA*., 1999, **96**, 3670-3675.

44. Y. Dai, D. Yang, P. Ma, X. Kang, X. Zhang, C. Li, Z. Hou, Z. Cheng, J. Lin, *Biomaterials*., 2012, **33**, 8704-8713.

45. C. Wang, L. Cheng, and Z. Liu, *Biomaterials*., 2011, **32**, 1110-1120.

46. C. F. Thorn, C. Oshiro, S. Marshe, T. H. Boussard, H. McLeod, T. E. Klein, and R. B. Altman, *Pharmacogenet Genomics*., 2011, **21**, 440-446.

47. A. Hekmat, A. A. Saboury, and A. Divsalar, *J. Biomed. Nanotechnol*., 2012, **8**, 968-982.

48. H. T. Wong, H. L. W. Chan, and J. H. Hao, *APPLIED PHYSICS LETTERS*., 2009, **95**, 0225121-3.

49. H. T. Wong, M. K. Tsang, C. F. Chan, K. L. Wong, B. Feic and J. Hao, *Nanoscale*., 2013, **5**, 3465-3473.

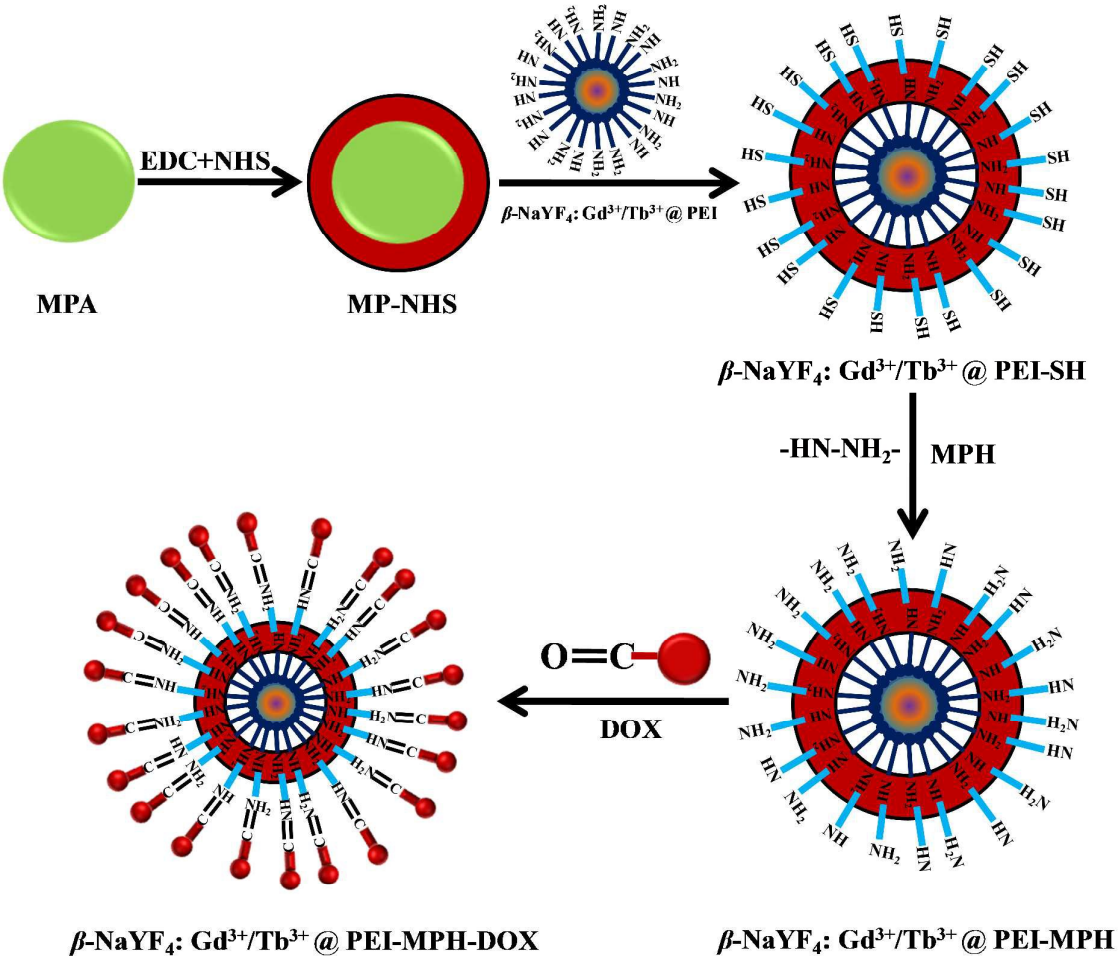

Scheme 1: Schematic illustration of the synthesis route for the conjugation of doxorubicin with β-$NaYF_4$: Gd^{3+}/Tb^{3+} nanorods via pH-sensitive hydrazone bond through MPH for pH-triggered drug delivery system.

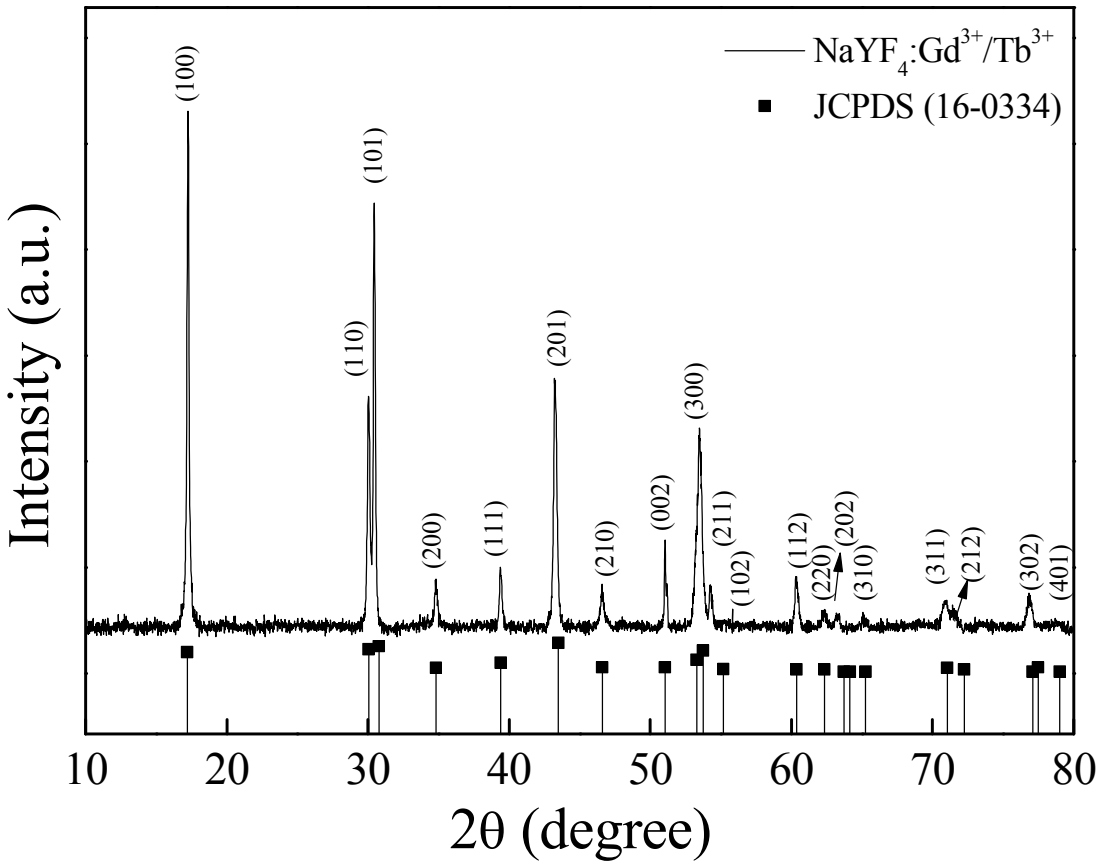

Figure 1: The comparison of XRD patterns of as-prepared β-$NaYF_4$: Gd^{3+}/Tb^{3+} nanorods and the reference data of hexagonal β-$NaYF_4$ (JCPDS- 16-0334) plotted as a reference. The overall peak profile demonstrates an excellent crystallinity of the nanorods.

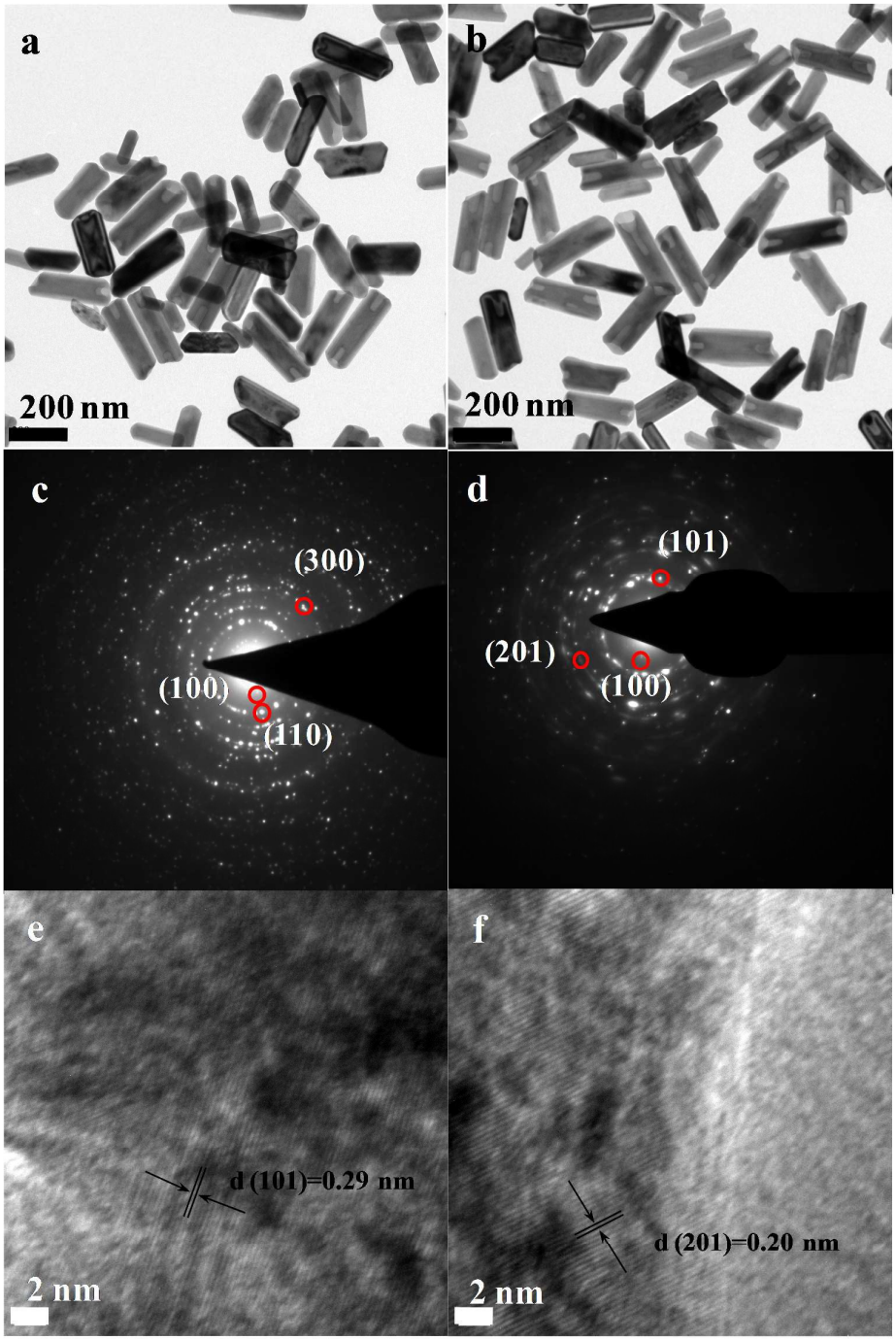

Figure 2: TEM images of (a) PEI-capped β-$NaYF_4$:Gd^{3+}/Tb^{3+} nanorods and (b) DOX – conjugated PEI capped β-$NaYF_4$:Gd^{3+}/Tb^{3+} nanorods. (c, d) and (e, f) are corresponding SAED patterns and HRTEM images. The nanorods are highly crystalline and well-separated even after drug conjugation.

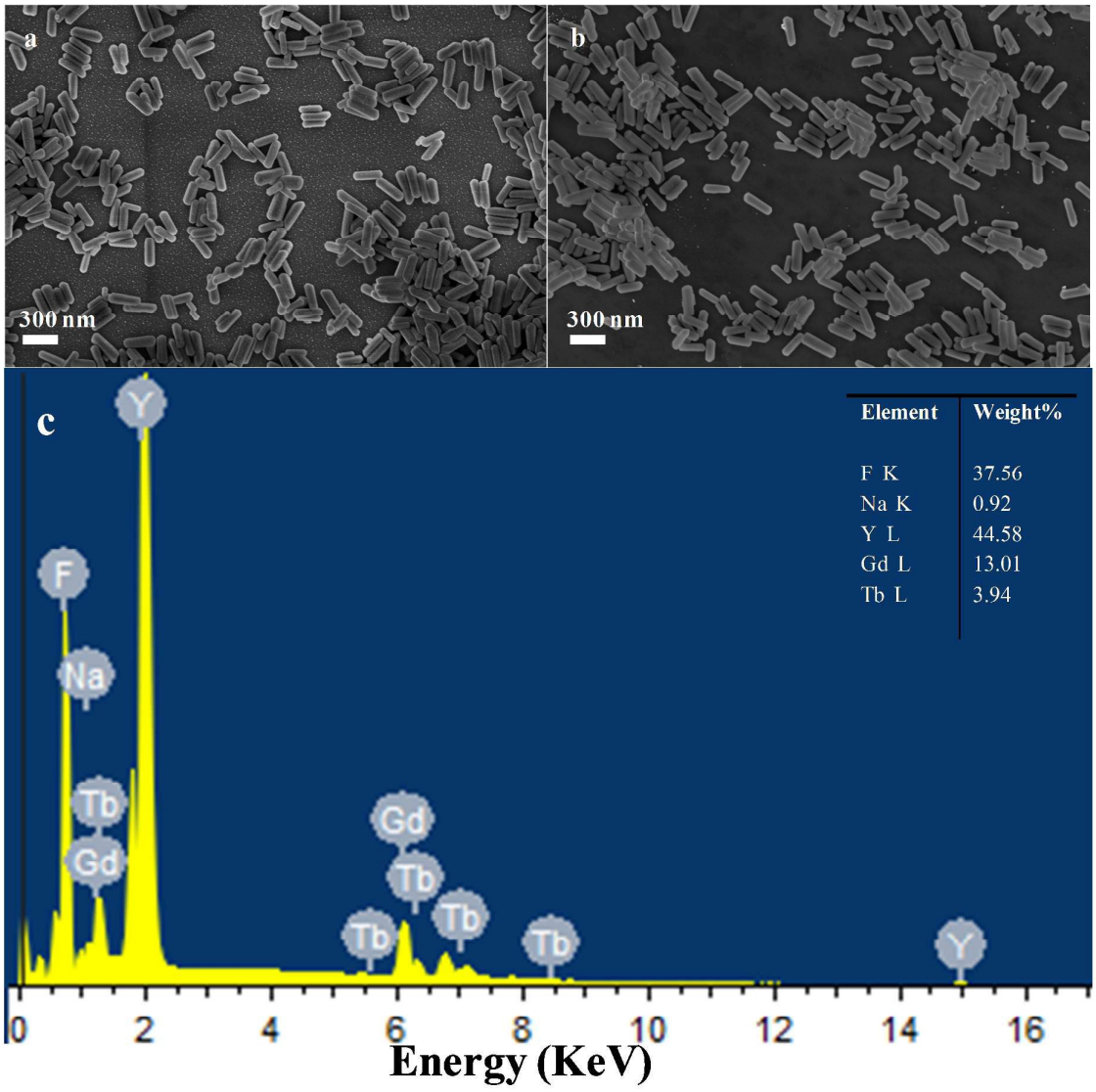

Figure 3: SEM images of (a) PEI capped β-$NaYF_4$:Gd^{3+}/Tb^{3+} nanorods and (b) DOX – conjugated β-$NaYF_4$:Gd^{3+}/Tb^{3+} nanorods. The rods remain nicely separated and monodispersed. (c) Energy-dispersive X-ray analysis (EDX) patterns of β- $NaYF_4$:Gd^{3+}/Tb^{3+} nanorods showing elemental composition.

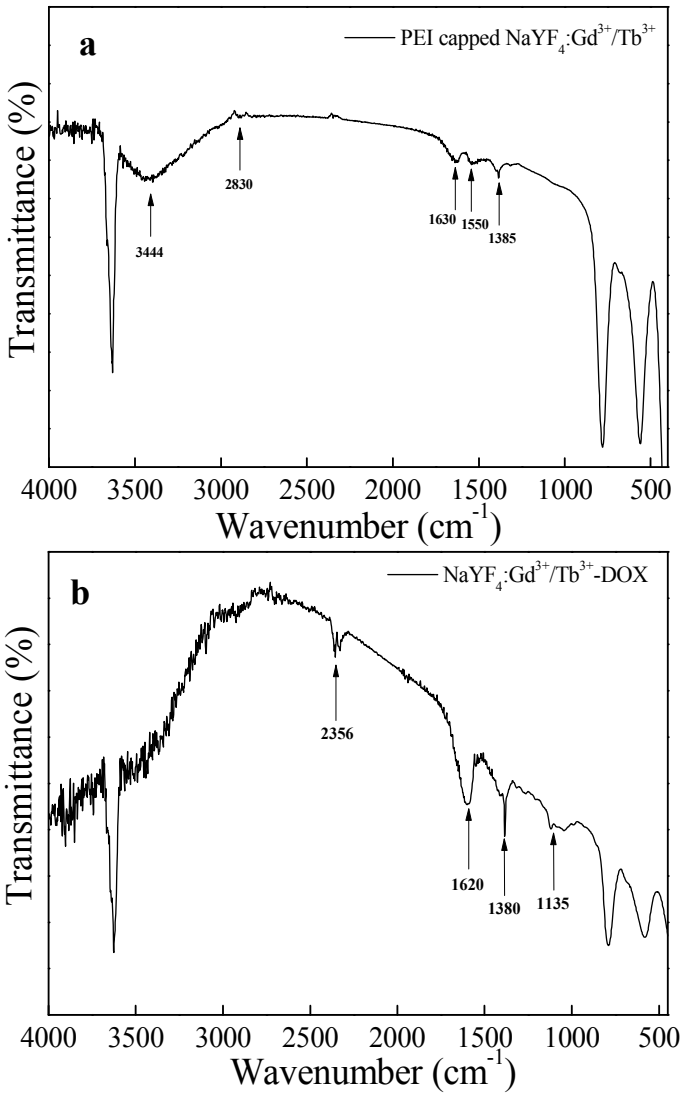

Figure 4: The FT-IR spectra of (a) PEI-capped β-$NaYF_4$:Gd^{3+}/Tb^{3+} nanorods and (b) DOX - conjugated β-$NaYF_4$:Gd^{3+}/Tb^{3+} nanorods indicating the capping of PEI at the surface of β-$NaYF_4$:Gd^{3+}/Tb^{3+} nanorods and further the conjugation of DOX with the amine functionalized β-$NaYF_4$:Gd^{3+}/Tb^{3+} nanorods.

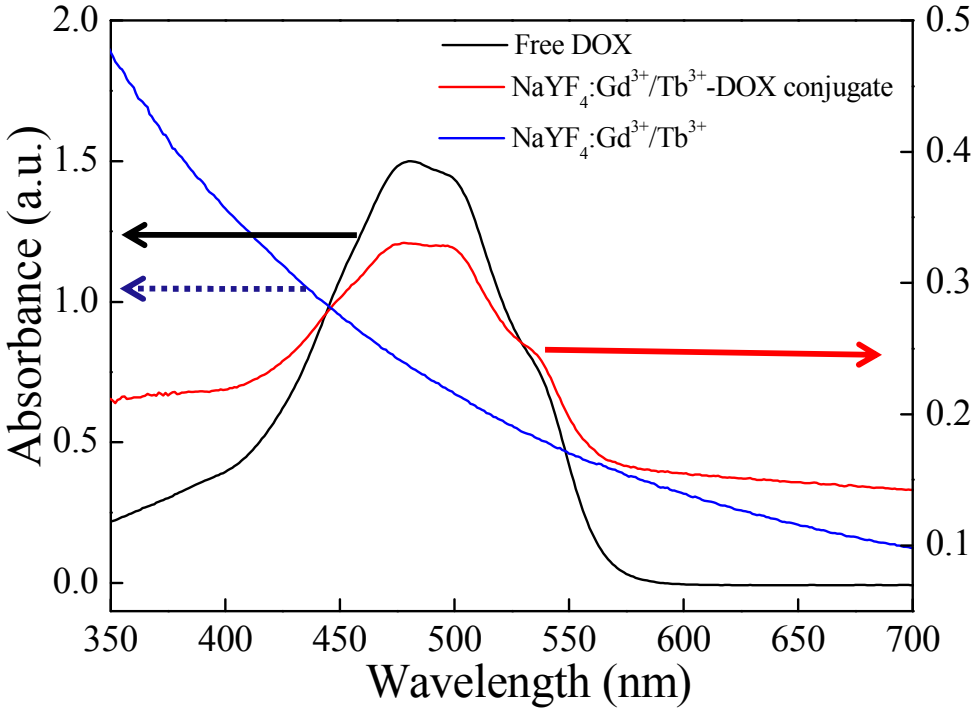

Figure 5: Comparison of UV-vis absorbance of free DOX, bare β-$NaYF_4$: Gd^{3+} / Tb^{3+} nanorods and β-$NaYF_4$:Gd^{3+}/Tb^{3+}- DOX conjugate nanorods indicating conjugation of DOX with β-$NaYF_4$:Gd^{3+}/Tb^{3+} nanorods.

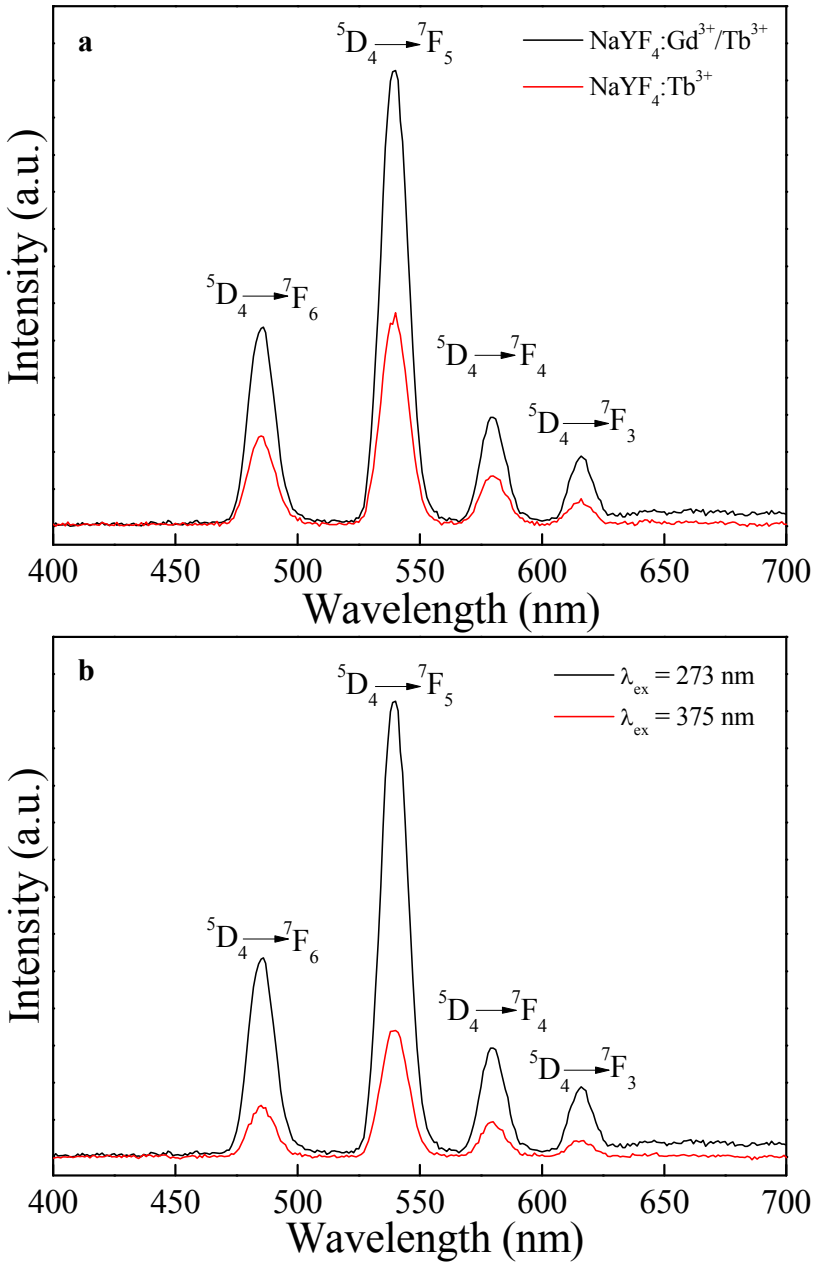

Figure 6: The comparison of static photoluminescence spectra showing the effect of sensitizer Gd^{3+} on the emission intensity. (a) Emission spectra of β-$NaYF_4$:5 % Tb^{3+} nanorods (red curve) at λ_{ex}= 375 nm and emission spectra of β-$NaYF_4$:Gd^{3+}/Tb^{3+} nanorods (black curve) at λ_{ex}= 273 nm. (b) Comparative emission spectra of β-$NaYF_4$:Gd^{3+}/Tb^{3+} nanorods at λ_{ex}= 273 nm and at λ_{ex}= 375 nm respectively. Here the background of curves is normalized to compare the intensities with each other.

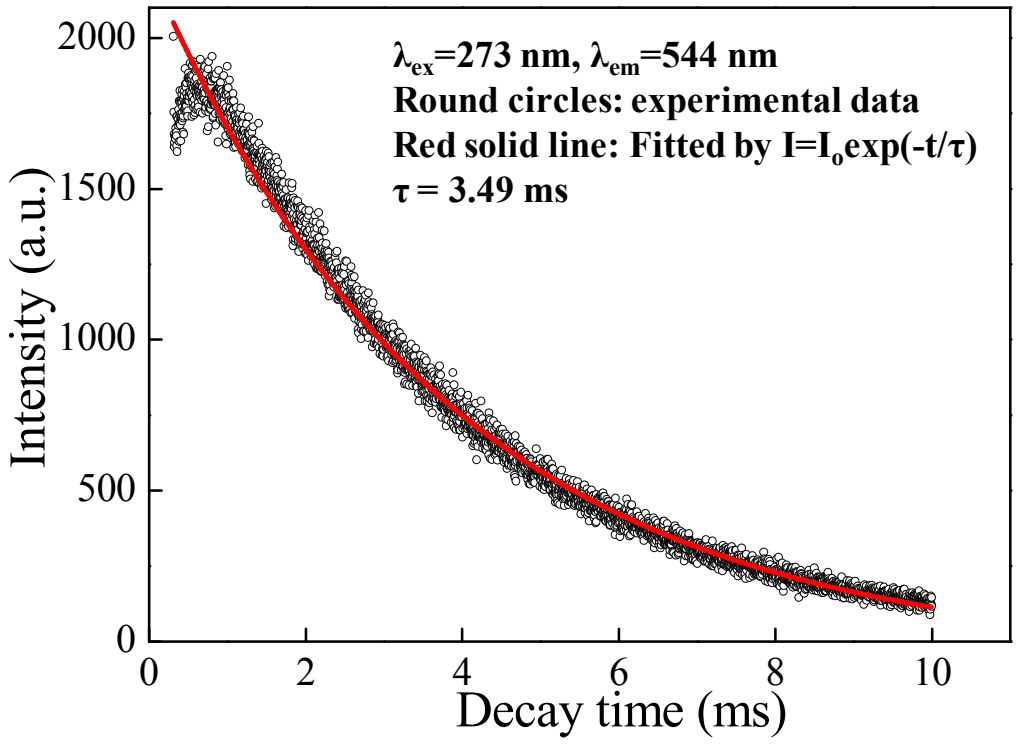

Figure 7: The luminescence decay curves for the $_5D^4 \rightarrow {}_7F^5$ emission of Tb^{3+} (λ_{ex}=273 nm, λ_{em}=544 nm) in β-$NaYF_4$:Gd^{3+}/Tb^{3+} nanorods.

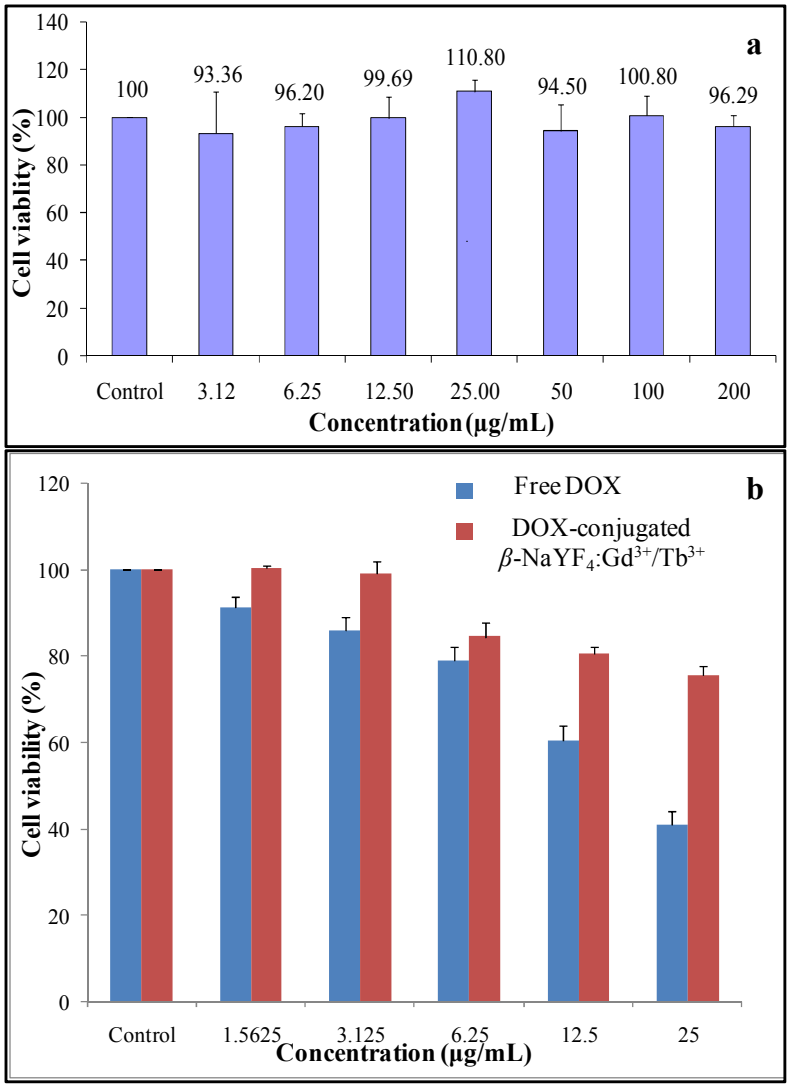

Figure 8: MTT assay showing the cytotoxicity of (a) the PEI-coated β-$NaYF_4$: Gd^{3+}/Tb^{3+} nanorods, and (b) Free DOX and DOX-conjugated β-$NaYF_4$: Gd^{3+}/Tb^{3+} in NIH3T3 cells by incubating them with NIH3T3 cells at 37 °C for 24 h.

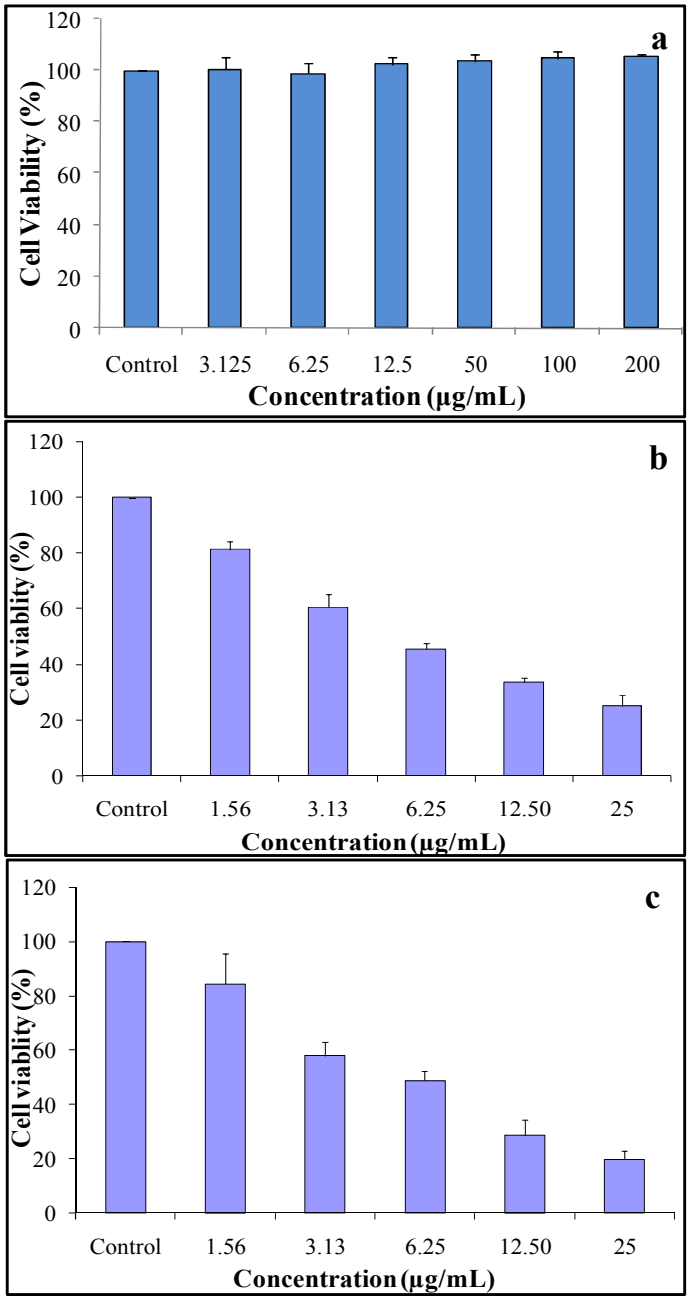

Figure 9: *In vitro* MCF-7 cancer cell viabilities after incubation of 24 h with (a) β-$NaYF_4$: Gd^{3+}/Tb^{3+} nanorods, (b) free DOX and (c) DOX-conjugated β-$NaYF_4$: Gd^{3+}/Tb^{3+}nanorods at different concentrations. DOX conjugated β-$NaYF_4$: Gd^{3+}/ Tb^{3+} nanorods exhibit an increasing inhibition against MCF-7 cancer cells with increasing concentration, while β-$NaYF_4$: Gd^{3+}/ Tb^{3+} nanorods do not possess toxicity to cancer cells.

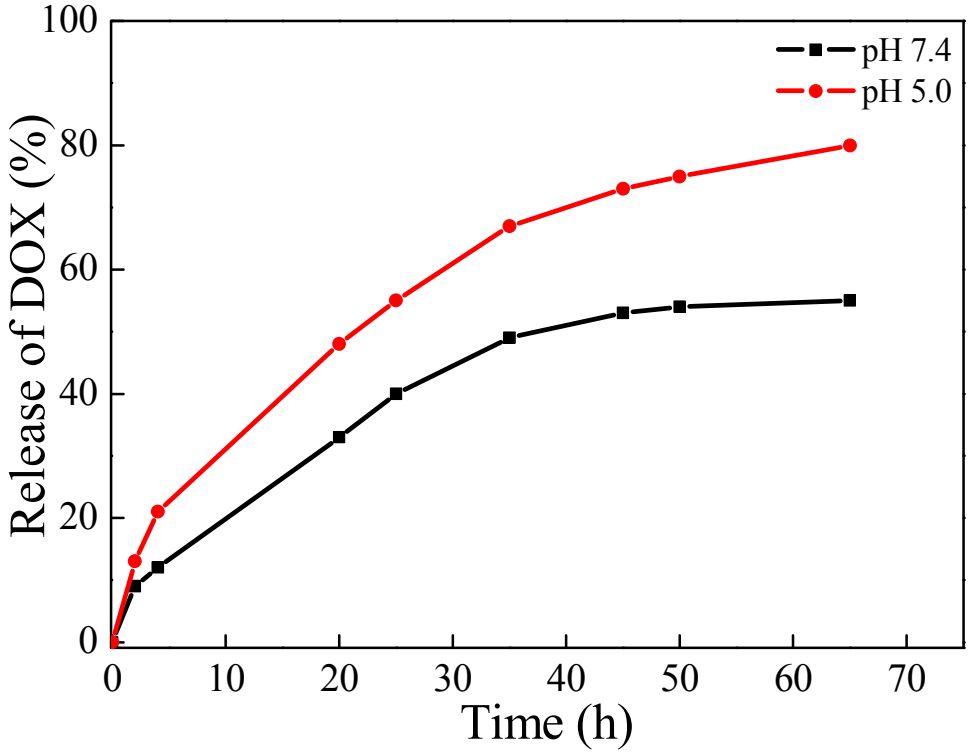

Figure 10: DOX release from DOX-conjugated β-$NaYF_4$: Gd^{3+}/Tb^{3+} nanorods over the period of time in PBS buffer at pH 7.4 and pH 5.0. The DOX release rate at acidic pH i.e. at pH 5.0 is much faster than that at pH 7.4 due to cleavage of pH-sensitive hydrazone bond linkage at pH 5.0.

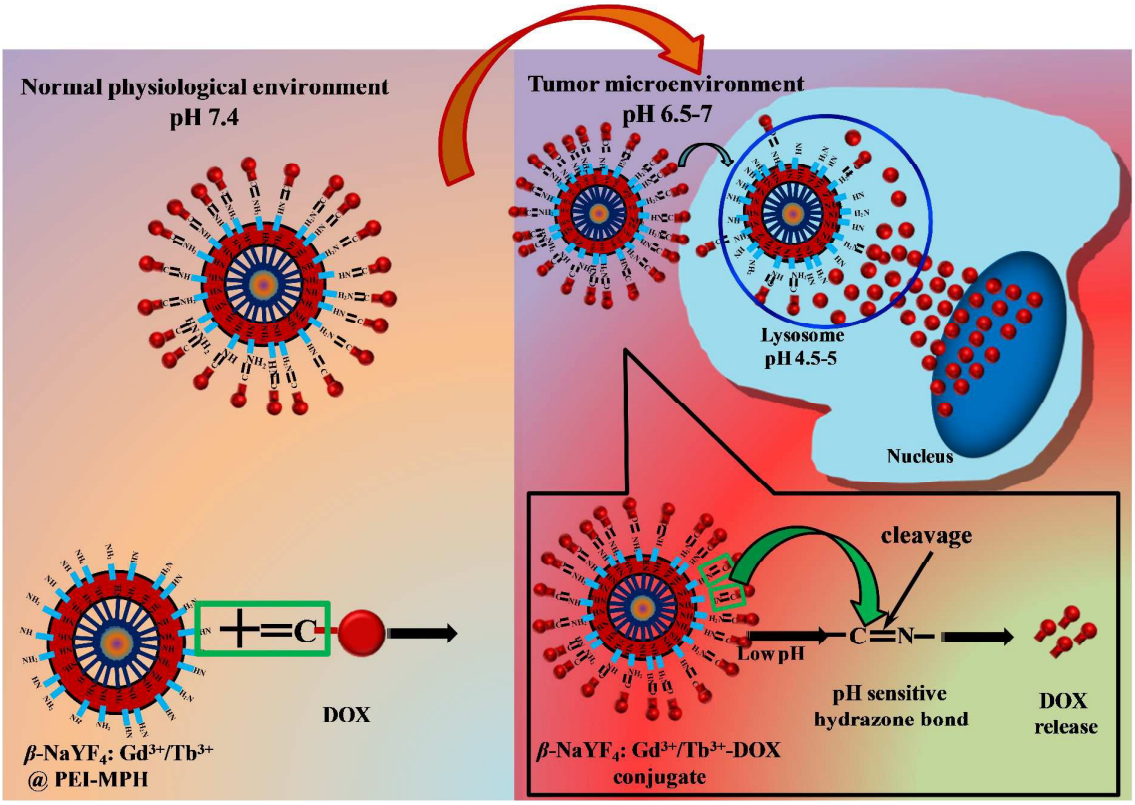

Scheme 2: A schematic representation of pH-triggered drug delivery system of DOX-conjugated β-$NaYF_4$:Gd^{3+}/Tb^{3+} nanorods showing the release of DOX inside the tumor cells via cleavage of pH sensitive hydrazone bond linkage at lysosomes (pH 4.5-5) and consequent internalization into the cells.

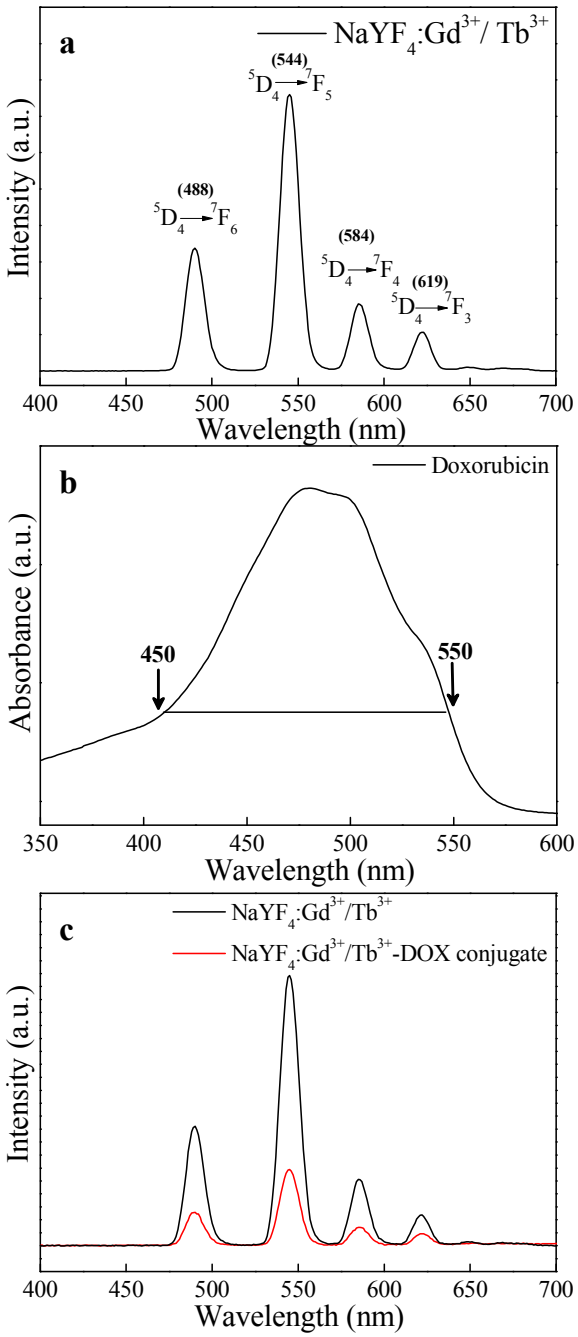

Figure 11: (a) The photoluminescence emission spectra of β-$NaYF_4$:Gd^{3+}/Tb^{3+} at λ_{ex}= 273 nm, and (b) the UV-vis absorption spectra of DOX showing a spectral overlap. (c) A comparison of the photoluminescence emission spectra of bare β-$NaYF_4$:Gd^{3+}/Tb^{3+} nanorods, and β-$NaYF_4$:Gd^{3+}/Tb^{3+}- DOX conjugates taken in same concentrations. It is seen that due to FRET mechanism the emission intensity of phosphor nanorods comes down after conjugation with DOX.

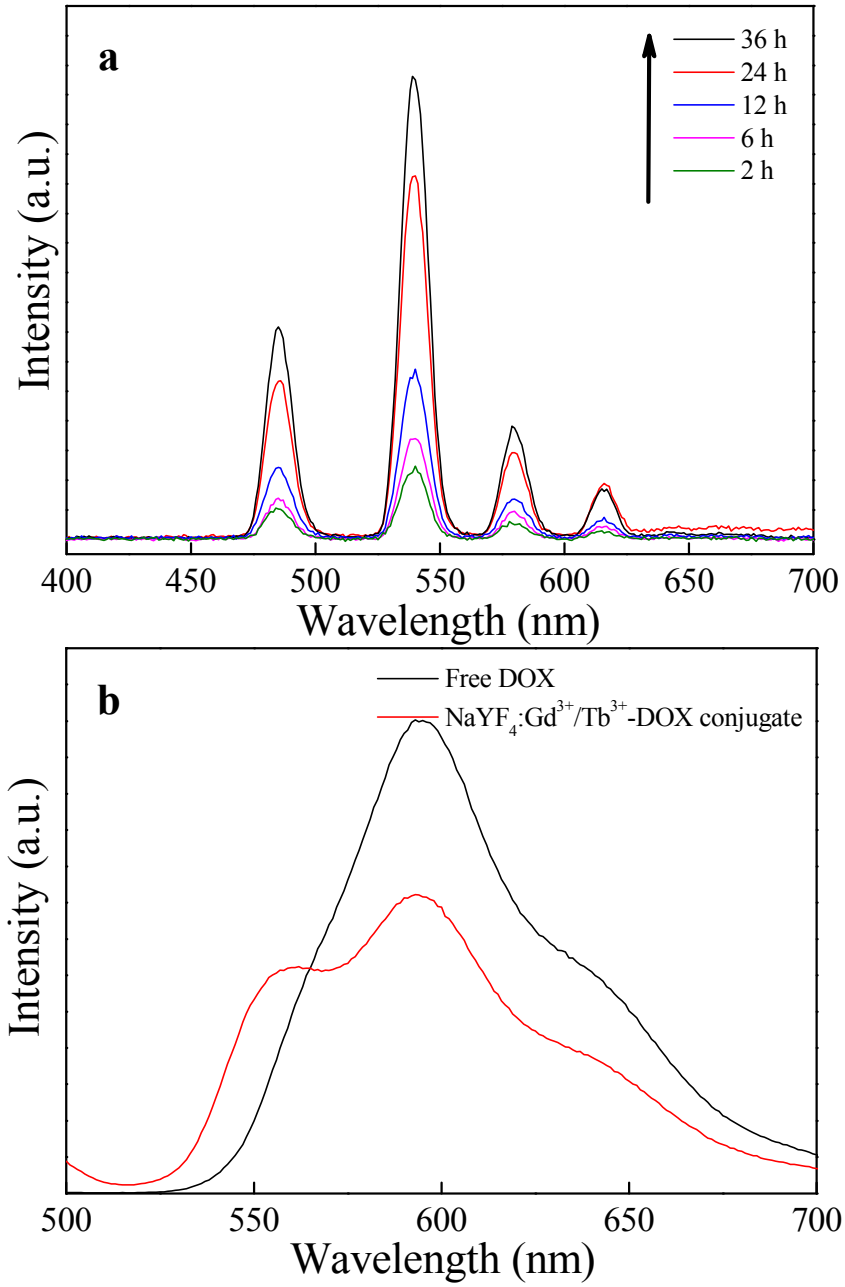

Figure 12: (a) The photoluminescence emission intensity of DOX conjugated - *β*-$NaYF_4:Gd^{3+}/Tb^{3+}$ nanorods as a function of DOX-release time at pH 5 and 37 °C in PBS buffer showing recovery of photoluminescence along with the release of DOX with increasing time by disabling FRET and (b) Photoluminescence spectra of free DOX and *β*-$NaYF_4:Gd^{3+}/Tb^{3+}$- DOX conjugate solutions.

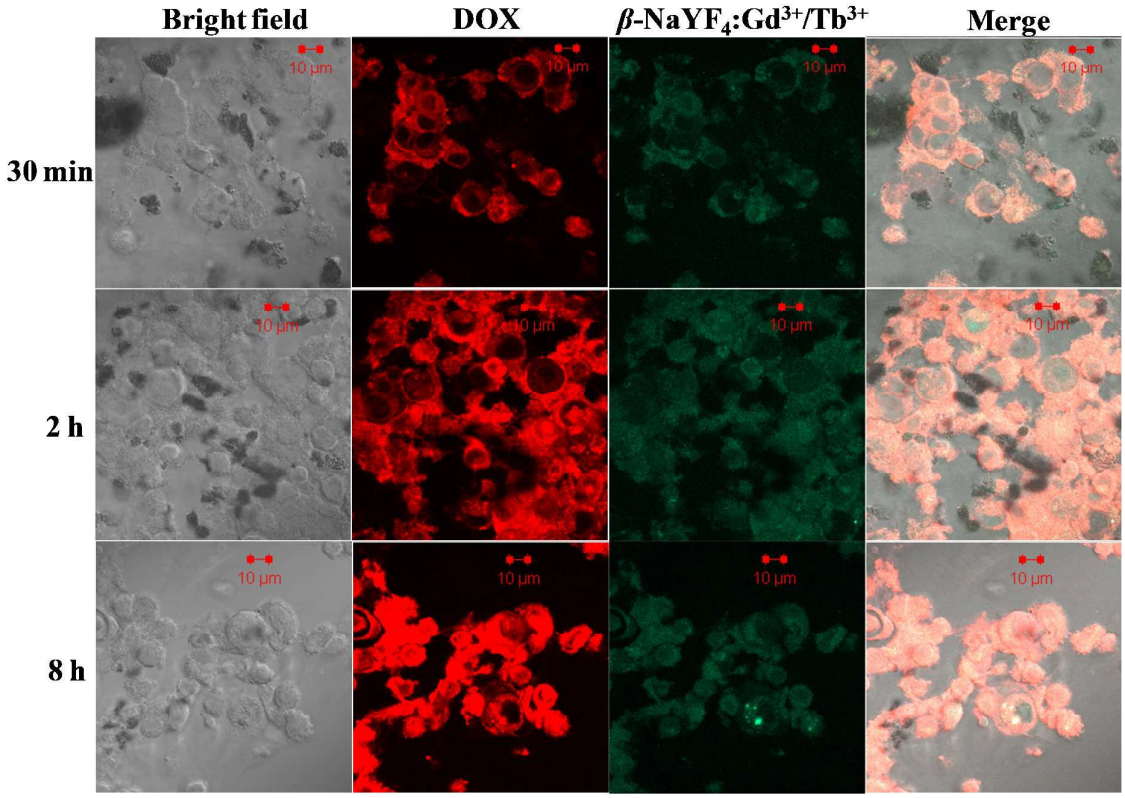

Figure 13: Confocal laser scanning microscopy (CLSM) images of MCF-7 cancer cells incubated with DOX-conjugated β-$NaYF_4$:Gd^{3+}/Tb^{3+} nanorods for 30 min, 2 h, and 8 h, at 37 °C. Emissions from β-$NaYF_4$:Gd^{3+}/Tb^{3+} (green colored) and DOX fluorescence (red colored) were recorded in the wavelength ranges of 500-550 nm and 500-600 nm. The scale bar is 10 μm.

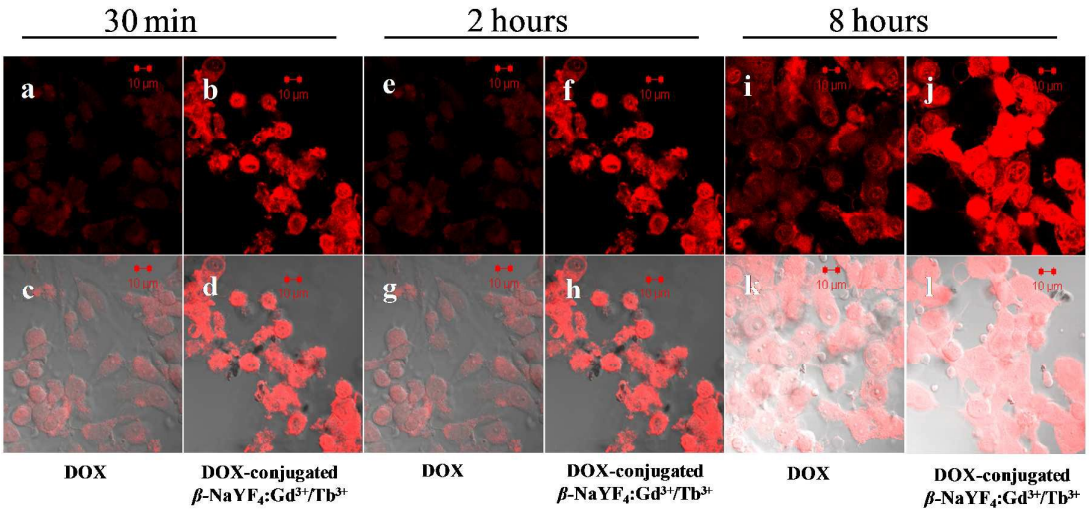

Figure 14: Cellular uptake of free doxorubicin in MCF-7 cancer cells at 30 min (a, c), 2 h (e, g), 8 h (i, k), and DOX-conjugated β-$NaYF_4$:Gd^{3+}/Tb^{3+} at 30 min (b, d), 2 h (f, h), 8 h (j, l), at pH 6.5, 37 °C. The lower row is corresponding merge images.

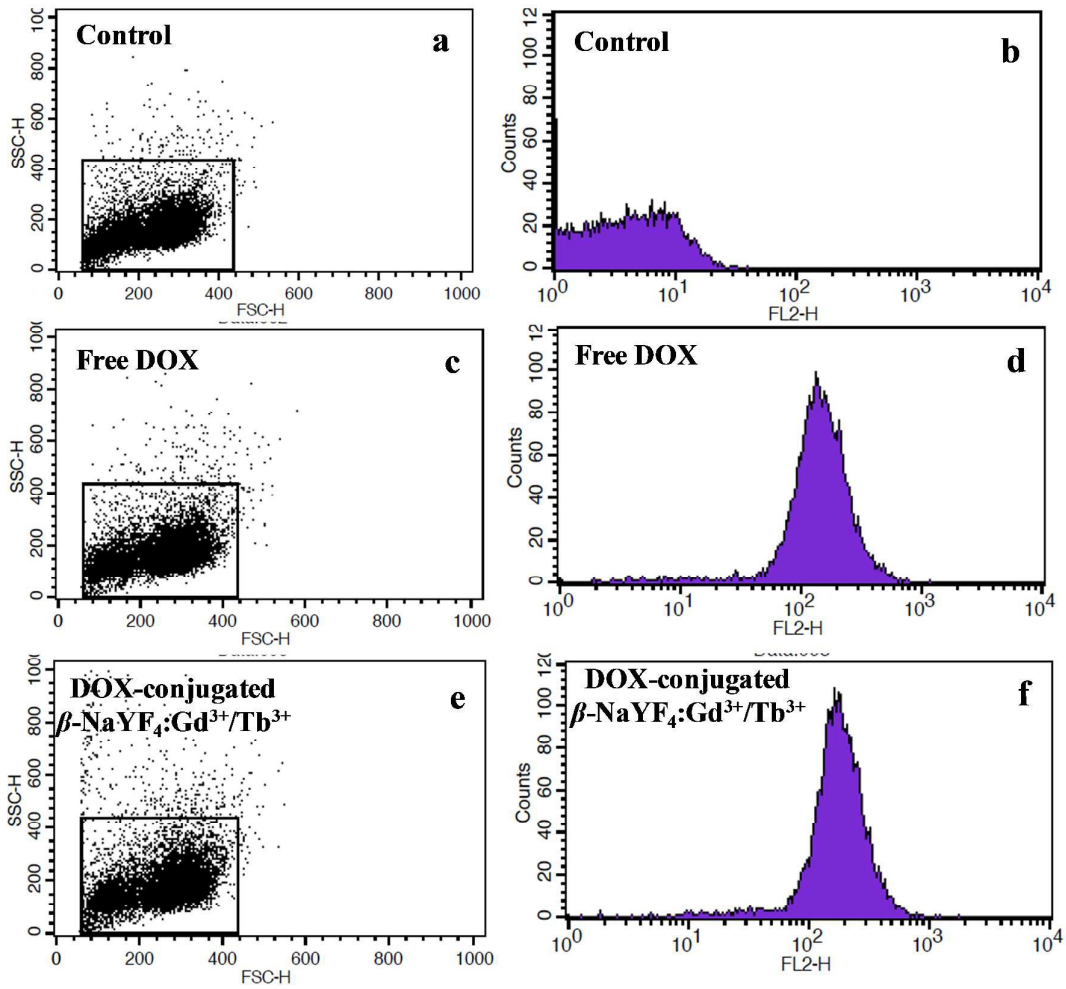

Figure 15: Flow cytometry analysis of MCF-7 breast cancer cells. (a, b) the control cells, (c, d) incubated with free DOX and, (e, f) incubated with DOX-conjugated β-$NaYF_4$:Gd^{3+}/Tb^{3+} nanorods for 4 h demonstrating the uptake of DOX conjugated β-$NaYF_4$: Gd^{3+}/ Tb^{3+} by the MCF-7 cells.

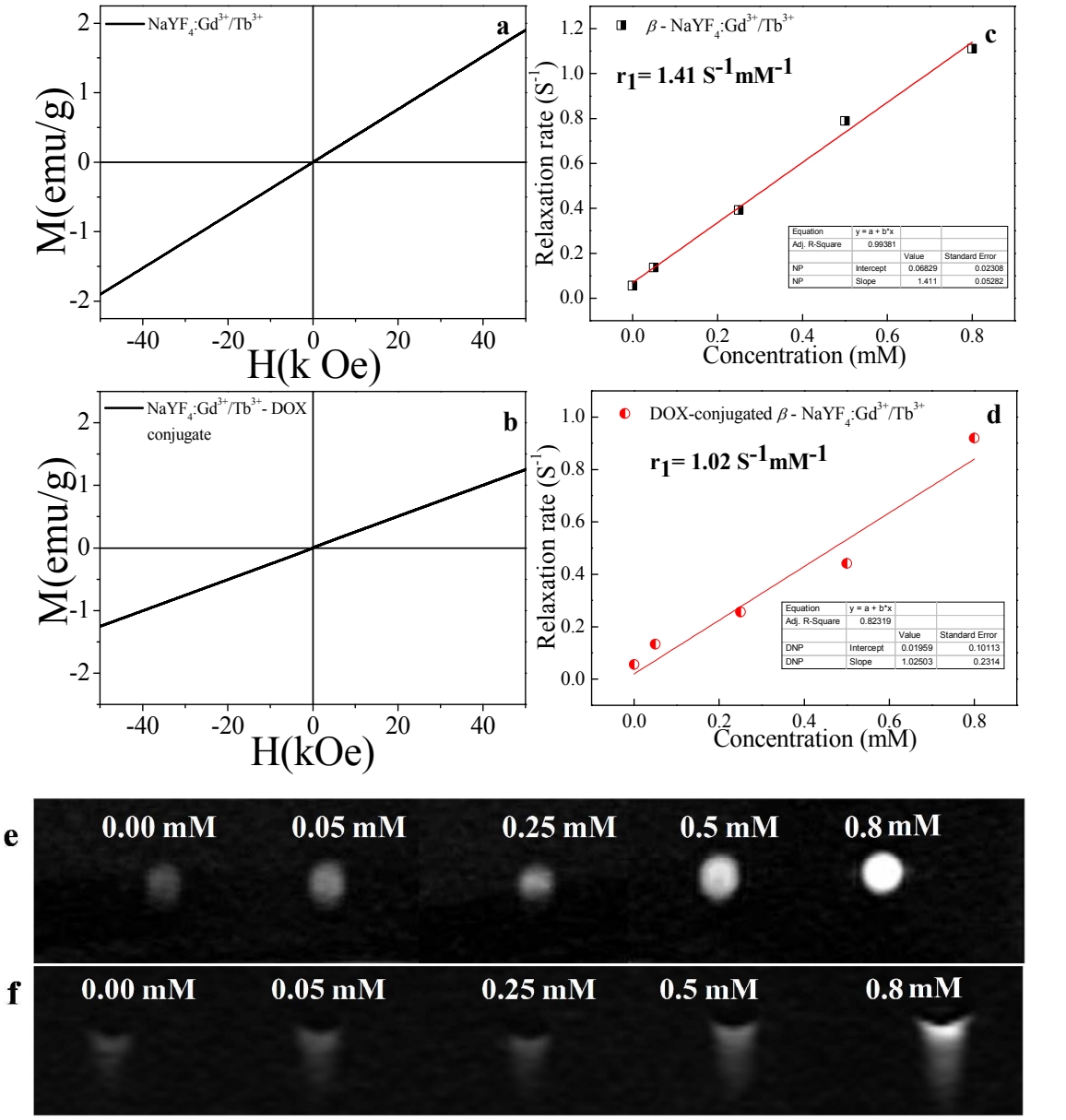

Figure 16: Magnetization as a function of applied field for (a) β-$NaYF_4$:Gd^{3+}/Tb^{3+} nanorods and (b) β-$NaYF_4$:Gd^{3+}/Tb^{3+}- DOX conjugate at room temperature showing paramagnetic behavior. The plot of ^1H spin-lattice relaxation rate ($1/T_1$) as a function of molar concentration (mM) of (c) β-$NaYF_4$:Gd^{3+}/Tb^{3+} nanorods and (d) β-$NaYF_4$:Gd^{3+}/Tb^{3+}- DOX conjugate at RT and 9.4 T. T_1 weighted MRI images of (e) β-$NaYF_4$:Gd^{3+}/Tb^{3+} nanorods and (f) β-$NaYF_4$:Gd^{3+}/Tb^{3+}- DOX conjugate at various molar concentrations in water. Deionised water (0.00 mM) was taken as reference.

TOC